



Cloud cover increase with increasing aerosol absorptivity: A counterexample to the conventional semidirect aerosol effect

Jan Perlwitz^{1,2} and Ron L. Miller^{1,2}

Received 10 June 2009; revised 18 September 2009; accepted 6 October 2009; published 27 April 2010.

[1] We reexamine the aerosol semidirect effect using a general circulation model and four cases of the single-scattering albedo of dust aerosols. Contrary to the expected decrease in low cloud cover due to heating by tropospheric aerosols, we find a significant increase with increasing absorptivity of soil dust particles in regions with high dust load, except during Northern Hemisphere winter. The strongest sensitivity of cloud cover to dust absorption is found over land during Northern Hemisphere summer. Here even medium and high cloud cover increase where the dust load is highest. The cloud cover change is directly linked to the change in relative humidity in the troposphere as a result of contrasting changes in specific humidity and temperature. More absorption by aerosols leads to larger diabatic heating and increased warming of the column, decreasing relative humidity. However, a corresponding increase in the specific humidity exceeds the temperature effect on relative humidity. The net effect is more low cloud cover with increasing aerosol absorption. The higher specific humidity where cloud cover strongly increases is attributed to an enhanced convergence of moisture driven by dust radiative heating. Although in some areas our model exhibits a reduction of low cloud cover due to aerosol heating consistent with the conventional description of the semidirect effect, we conclude that the link between aerosols and clouds is more varied, depending also on changes in the atmospheric circulation and the specific humidity induced by the aerosols. Other absorbing aerosols such as black carbon are expected to have a similar effect.

Citation: Perlwitz, J., and R. L. Miller (2010), Cloud cover increase with increasing aerosol absorptivity: A counterexample to the conventional semidirect aerosol effect, *J. Geophys. Res.*, 115, D08203, doi:10.1029/2009JD012637.

1. Introduction

[2] Owing to the high spatial and temporal variability of tropospheric aerosols such as soil (or “mineral”) dust, their net effect on the radiation balance of the atmosphere and on climate is still highly uncertain [Forster *et al.*, 2007]. Tropospheric aerosols change the radiation balance directly by absorbing and reflecting radiation in solar and thermal wavelengths (for a review, see Satheesh and Moorthy [2005] and Forster *et al.* [2007]), and indirectly through microphysical interaction between water droplets and aerosol particles, which act as cloud condensation nuclei (CCN). The microphysical effect of aerosols is thought to increase cloud albedo by increasing the cloud droplet number concentration [Twomey, 1977], cloud lifetime [Albrecht, 1989], and cloud height [Pincus and Baker, 1994]. Despite the high complexity and nonlinearity of the microphysical interaction between aerosols and clouds, modeling studies generally indicate that the net effect of this interaction is to reflect more radiation back to outer space [Forster *et al.*, 2007], although recent

results show that aerosols acting as ice nuclei could counteract the cooling effect significantly [Storelvmo *et al.*, 2008]. A few observational studies seem to confirm a relation between soil dust aerosols and cloud cover. Observations during a dust storm suggested smaller cloud droplets and suppressed precipitation over the eastern Mediterranean [Rosenfeld *et al.*, 2001]. Observed thin low cloud amount and mineral dust showed a positive correlation off the west coast of North Africa, where soil dust is abundant [Mahowald and Kiehl, 2003]. In another study, rainfall and dust load in the West African Sahel exhibited a negative correlation, which was explained by a larger number of CCN when the dust load is high, distributing available cloud water over a larger number of droplets, thus suppressing droplet growth and precipitation [Hui *et al.*, 2008].

[3] An additional, hypothesized effect of absorbing tropospheric aerosols is the semidirect effect [Grassl, 1975; Hansen *et al.*, 1997a; Ackerman *et al.*, 2000]. Absorbing aerosols are thought to warm the layer in which they are located, leading to decreased relative humidity and less cloud cover. This effect can increase the amount of solar radiation that reaches Earth’s surface and is absorbed, leading to additional warming and a further decrease in the cloud amount. Some observations are consistent with the semidirect effect. Koren *et al.* [2004] measured reduced cloud formation in the Amazon region and linked this to smoke from biomass burning using a one-dimensional

¹Department of Applied Physics and Applied Mathematics, Columbia University, New York, New York, USA.

²NASA Goddard Institute for Space Studies, New York, New York, USA.

radiation transfer model. A modeled cloud cover decrease over eastern Germany during an observed Saharan dust outbreak has also been interpreted as the semidirect effect by absorbing dust [Helmert *et al.*, 2007], as has a reduction of cloud cover over East Asia inferred from satellite retrievals [Huang *et al.*, 2006].

[4] Using a large-eddy model that excluded microphysical interaction, Johnson *et al.* [2004] simulated a significantly reduced marine stratocumulus liquid water path by absorbing aerosols in the boundary layer. The semidirect effect of aerosols upon clouds was significantly stronger than the direct radiative effect of the aerosols and was proportional to the single-scattering albedo. However, when the warming aerosol layer was located above the cloud layer, cloud cover increased; that is, the semidirect effect reversed in sign. Studies using general circulation models (GCMs) exhibit a positive semidirect effect leading to reduced low cloud cover and a drier climate [Cook and Highwood, 2004; Ramanathan *et al.*, 2005]. A recent study concludes that the magnitude of the semidirect effect on marine stratocumulus clouds depends nonlinearly on the CCN concentration of black carbon aerosols and is significantly enhanced for high CCN concentrations [Hill and Dobbie, 2008]. A reduction of deep convective clouds with increasing absorptivity of aerosols in the two-dimensional cloud-resolving Goddard cloud ensemble model with spectral bin cloud microphysics has been attributed to the semidirect effect as well [Fan *et al.*, 2008].

[5] Results from other studies suggest that large-scale circulation changes due to absorbing aerosols could strongly modify the semidirect effect, which was originally conceived as a local thermodynamical effect. In a GCM study by Menon *et al.* [2002] on the climate effect of black carbon aerosols, a low cloud cover increase was detected over Asia and the Indian Ocean related to an uplifting of air heated by the absorbing aerosols. Miller *et al.* [2004] found that low cloud cover and precipitation were increased by dust radiative forcing over the western Sahara desert. They hypothesized that in an arid region, where the column moisture is low and the atmospheric radiative cooling is weak, a modest atmospheric heat anomaly by dust radiative forcing could change the sign of total diabatic heating, resulting in ascent and precipitation. The cloud cover and precipitation anomalies increased with dust absorption in contradiction to the conventional understanding of the semidirect effect, described, e.g., by Hansen *et al.* [1997a]. However, the exact causal relationship behind these modeled changes remains unknown.

[6] In our study, we reexamine the effect of absorbing tropospheric aerosols upon clouds in the atmospheric GCM used by Miller *et al.* [2004] in order to better understand the causal relationship between cloud cover and radiative forcing by absorbing aerosols. We diagnose the changes in specific and relative humidity using the moisture budget. We show that a moisture increase in the atmosphere warmed by the absorbing dust aerosols can overcome the decrease in relative humidity due to the heating, particularly in the lower troposphere. Diabatic heating by dust aerosols can increase moisture convergence, leading to a significant increase in low cloud cover and under certain conditions even in medium and high cloud cover. One goal is to determine whether the cloud cover increase exhibited by the model is limited to

dust absorption or whether the mechanism might be expected to apply to other absorbing aerosols such as black carbon.

[7] After describing the design of the experiments in section 2 and the radiative forcing in section 3, we present the cloud cover changes observed in our simulations and their dependence on the single-scattering albedo (SSA) in section 4. In sections 5 and 6, we analyze the relationship between the cloud cover response and the moisture change (section 5) and their relationship to evaporation, precipitation, and water vapor convergence (section 6). The changes in the general circulation due to dust radiative forcing and how they are linked to the cloud cover changes are discussed in more detail in section 7. A summary and conclusions are presented in section 8.

2. Atmospheric GCM and the Experimental Design

[8] The atmospheric GCM used for our transient simulations is the Goddard Institute for Space Studies (GISS) SI2000 atmospheric model described in a study on climate forcings [Hansen *et al.*, 2002]. It has a horizontal resolution of 4° latitude by 5° longitude and 12 vertical layers. The strength and the deficiencies of the model have been discussed elsewhere [Hansen *et al.*, 1983, 1997b, 2002]. The model uses the prognostic scheme of Del Genio *et al.* [1996] for large-scale cloud parameterization, which follows the approach of Sundqvist *et al.* [1989]. The scheme of Del Genio and Yao [1993] is used for the convection parameterization. Radiative transfer in clouds is calculated on the basis of a single Gauss point (SGP) doubling/adding algorithm for homogenous plane-parallel clouds with semi-random cloud overlap [Hansen *et al.*, 1983]. To account for an inhomogeneous distribution of droplets within the cloud, a simple renormalization method provides adjusted mean single-scattering parameters and optical depth of the cloud, which are used to calculate the mean reflection and transmission of radiation with the SGP algorithm, as described by Cairns *et al.* [2000].

[9] The dust aerosol optical depth (AOD) in the model version we used was calculated off-line. The calculation of the dust radiative effect is described in more detail by Perlwitz *et al.* [2001] and Miller *et al.* [2004]. In summary, radiative parameters, such as the SSA, are calculated for eight size classes of soil dust particles distinguished by particle radius, of which four size classes are within the submicron range [Tegen and Lacis, 1996]. The SSA depends on the dust particle size and wavelength (e.g., 1 μm size, SSA = 0.86; 0.5 μm size, SSA = 0.92 at 0.55 μm wavelength for the baseline case). The radiative parameters for the different particle sizes are determined using Mie theory, where dust particles are approximated as perfect spheres. This causes a misestimation of the scattering phase function for dust particles. Although this is important for remote sensing applications, the idealization has little effect on the climate forcing, which is a hemispheric integral [Lacis and Mishchenko, 1995]. Radiative forcing, the perturbation to the solar and thermal radiative fluxes by the prescribed dust distribution in the absence of any feedbacks, or changes to the atmosphere, was calculated off-line using the radiative code of the atmospheric GCM, as described by Miller *et al.* [2004].

First, the atmospheric GCM was integrated without dust through one annual cycle using prescribed temperature, humidity, and cloud cover distributions archived every 5 h from a previous equilibrium simulation of a year 1951 atmosphere. Then the integration was repeated with the same distributions of these variables and the dust distribution used in our experiments to obtain the change in the radiation fluxes because of the presence of dust.

[10] Five sets of experiments were conducted in our study. Each set of simulations is an ensemble of 10 experiments. The experiments within each ensemble differ only regarding the atmospheric initial conditions that were randomly perturbed. The first ensemble, the “no-dust” case, was run without dust radiative forcing. Four additional ensembles were run with different dust radiative forcings. The radiative forcing by dust for each ensemble was calculated using a different range of the SSA in the solar range of the spectrum. We distinguish between a so-called baseline case, a more reflecting case, a more absorbing case, and a strongly absorbing case. The baseline case corresponds to the refractive indices provided by *Volz* [1973] and *Patterson and Gillette* [1977] on the basis of measurements of far-traveled Saharan dust particles, which were prescribed for dust from all source regions in the model. For the more reflecting ensemble of simulations, the SSA was increased by 10% but not to more than a value of 1 (purely reflecting) at each wavelength of solar radiation. For the more absorbing and the strongly absorbing ensemble of simulations, the SSA was decreased by 10% and 20%, respectively. Observed dust scattering and absorption coefficients depend on the mineralogical composition of the soil in the source region [*Dubovik et al.*, 2002; *Kubilay et al.*, 2003]. Mixing of hematite, which is highly absorbing, into dust aggregates can increase the absorptivity of dust particles significantly [*Sokolik and Toon*, 1999; *Mishra and Tripathi*, 2008]. There is a large uncertainty in observed coefficients because of discrepancies between in situ and satellite measurements [*Dubovik et al.*, 2002]. Thus, the SSA observed in some regions might even exceed the SSA range covered with our simulations, although our chosen range probably overestimates the uncertainty of the global average. In any case, our goal in this study is not to calculate the precise numerical change in cloud cover by dust radiative forcing. Instead, we want to use the sensitivity of the cloud anomalies to the aerosol SSA to understand the mechanism relating clouds and aerosols in the model.

[11] Forcing by other atmospheric constituents, such as greenhouse gases, volcanic sulfate aerosols in the stratosphere, ozone, stratospheric water vapor, tropospheric sulfates, and tropospheric carbonaceous aerosols, some of which were time-dependent, was prescribed identically in all experiments according to *Hansen et al.* [2002]. Thus, differences between the results from our different ensemble simulations are solely due to differences between the dust radiative forcing.

[12] Lower boundary conditions such as sea surface temperature and sea ice cover were calculated using a mixed layer ocean model with deep diffusion and a simple thermodynamic sea ice model, respectively. The ensemble simulations with perturbed initial conditions were started from an equilibrium state and run from the year 1951 to the year 2050.

[13] For our analyses, we calculated both the long-term seasonal averages over the full 100 simulated years (99 years for Northern Hemisphere winter) of each experiment and the ensemble means from the 10 members of each case. For variables such as temperature, specific humidity, and cloud cover, the response to dust radiative forcing is calculated as the difference between the ensemble means of the simulations with and without dust radiative forcing. Since some of the forcings other than the one by dust were time-dependent, we repeated our analyses for the basic model variables using detrended data. The results did not show any significant differences between both approaches. We show only results based on the first approach in sections 3–7.

3. Prescribed Distribution of Dust Radiative Forcing

[14] The dust AOD has a prescribed annual cycle but no interannual variability. The daily dust AOD values were interpolated from monthly average values, which were obtained from previous off-line calculations with a chemical transport model [*Tegen et al.*, 1997]. The seasonal averages of the dust AOD are shown in Figure 1. Comparisons of the simulated dust distribution with observations were performed in earlier studies [*Tegen and Fung*, 1995; *Tegen et al.*, 1997; *Miller et al.*, 2006]. The prescribed dust AOD has some biases. It is generally lower than observed over the Sahara and downwind over the Atlantic and North America, particularly in Northern Hemisphere summer. The magnitude and the annual cycle of the prescribed dust AOD show better agreement with observations over the Arabian Sea, although in July and August, the magnitude seems to be higher than observed. Again, we are interested in the dynamical mechanism linking cloud cover and forcing by absorbing aerosols, and the biases mentioned here are not expected to impact our conclusions.

[15] The top of atmosphere (TOA) radiative forcing in the four experimental sets with dust is shown in Figure 2 for the Northern Hemisphere winter and summer mean. Its geographical distribution depends on the single-scattering albedo of the dust aerosols but varies also with the surface albedo [*Chylek and Coakley*, 1974], e.g., land versus ocean [*Satheesh and Ramanathan*, 2000] and underlying clouds [*Podgorny and Ramanathan*, 2001; *Keil and Haywood*, 2003; *Chand et al.*, 2009]. For more reflecting dust, radiative forcing is negative over most areas of the globe with minimum values of about -5 to -7 and -20 to -26 W m^{-2} in areas with high dust AOD in winter and summer, respectively. When the SSA of dust particles is decreased, TOA forcing turns positive and its magnitude increases [see also *Tegen and Lacis*, 1996]. For strongly absorbing dust, during winter, a maximum forcing of about 5 to 9 W m^{-2} is found where the dust AOD is high, over North Africa and Australia. During summer, the magnitude of the forcing is even larger in a high-dust region that stretches from western North Africa, over the Arabian Peninsula to India. It amounts to between 20 and more than 50 W m^{-2} in the eastern part of this region for strongly absorbing dust. For more absorbing dust, the forcing is between 25 and 35 W m^{-2} . Stronger forcing is also located over East Asia in this season due to the dust sources located there and in northern high latitudes.

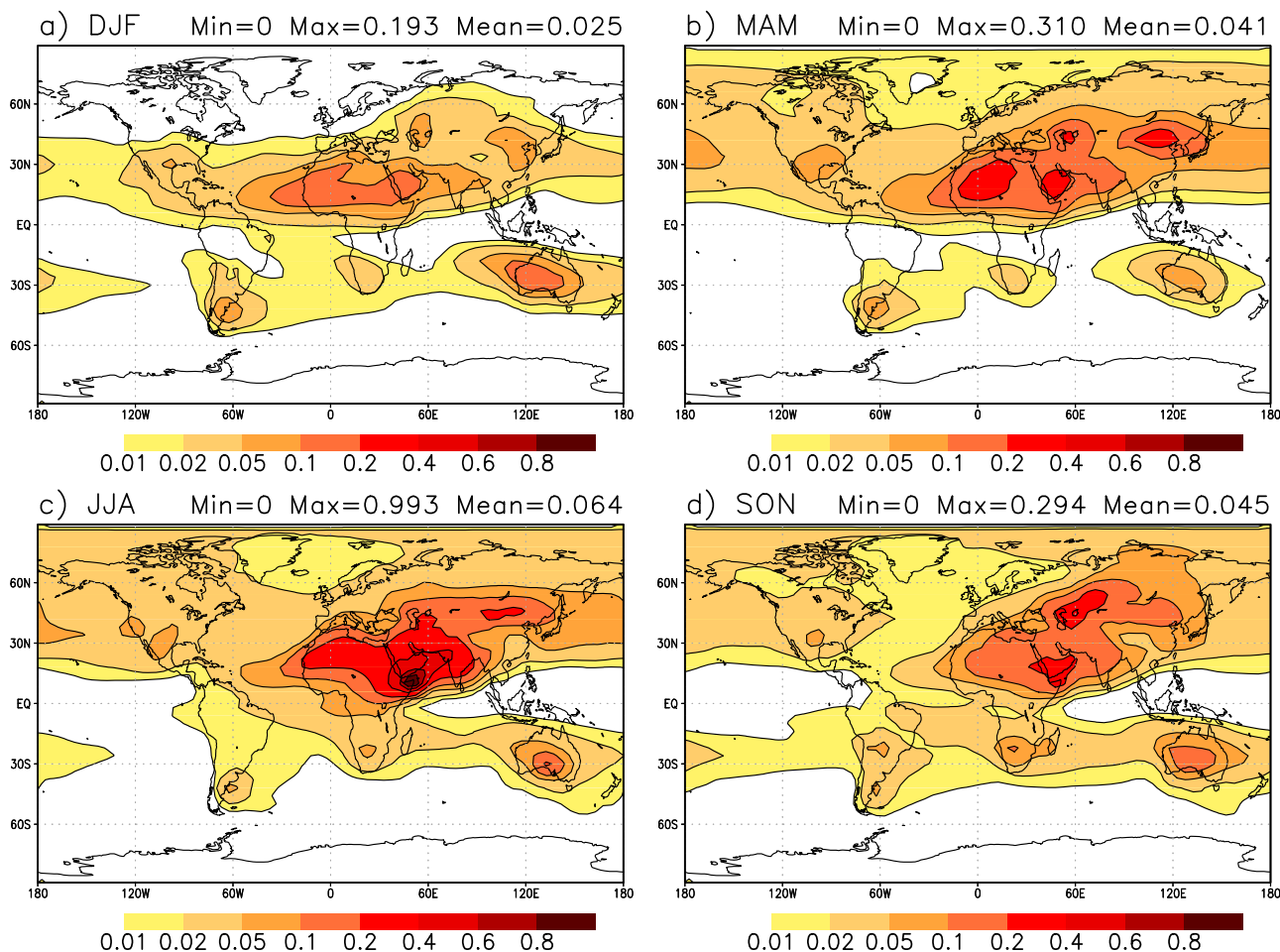


Figure 1. Seasonal means of prescribed dust aerosol optical depth at the wavelength of $0.55 \mu\text{m}$ in the ensemble simulations with dust radiative forcing for (a) Northern Hemisphere winter (DJF), (b) spring (MAM), (c) summer (JJA), and (d) fall (SON).

[16] The global average of the TOA dust radiative forcing (Table 1) changes accordingly from negative for more reflecting dust (-0.53 and -0.76 W m^{-2} in Northern Hemisphere winter and summer, respectively) to positive with increasing magnitude as the absorptivity of dust particles increases (corresponding to decreasing SSA), with the largest forcing in Northern Hemisphere summer, when the globally averaged dust AOD is highest, amounting to 1.5 and 2.77 W m^{-2} for more and strongly absorbing dust, respectively. The global average of the surface radiative forcing (Table 2) is negative in all simulations and increases in magnitude with increasing absorptivity of the dust aerosols. Again, its magnitude is largest in summer. Accordingly, the globally averaged heating of the atmosphere due to dust aerosols, as the difference between TOA and surface radiative forcing, amounts to 0.23 and 0.69 W m^{-2} in winter and summer, respectively, for more reflecting dust and increases to 2.97 and 7.1 W m^{-2} , respectively, for strongly absorbing dust. Although similar in magnitude, the globally and annually averaged values of both the TOA forcing and the radiative heating calculated in our study from a prescribed dust AOD are somewhat larger than in the study by Miller *et al.* [2004], who calculated the dust aerosol distribution interactively. A possible cause is that calculating dust

aerosols interactively with the GISS GCM reduces the global dust emission by about 15% compared to off-line calculations, since dust radiative forcing negatively feeds back on the dust emission by reducing wind speed at the surface, in turn reducing dust radiative forcing [Perlwitz *et al.*, 2001].

4. Cloud Cover Response to Dust Radiative Forcing

[17] The ensemble mean cloud cover response in our simulations is displayed in Figure 3 for each season as a function of TOA dust radiative forcing. Different values of the forcing result from variations in the prescribed SSA and are a measure of the initial imbalance in the energy flux between the Earth-atmosphere system and outer space due to both the absorbing and reflecting effect of dust on radiation. The globally averaged low cloud cover, which is shown in Figure 3a, increases in all seasons with increasing radiative forcing. The increase is nearly linear. The slope is somewhat smaller in Northern Hemisphere winter and spring than in summer and fall. This increase in low cloud cover with aerosol absorptivity is a counterexample to the commonly understood semidirect effect [Denman *et al.*, 2007]. In contrast, medium cloud cover (except in summer) and high

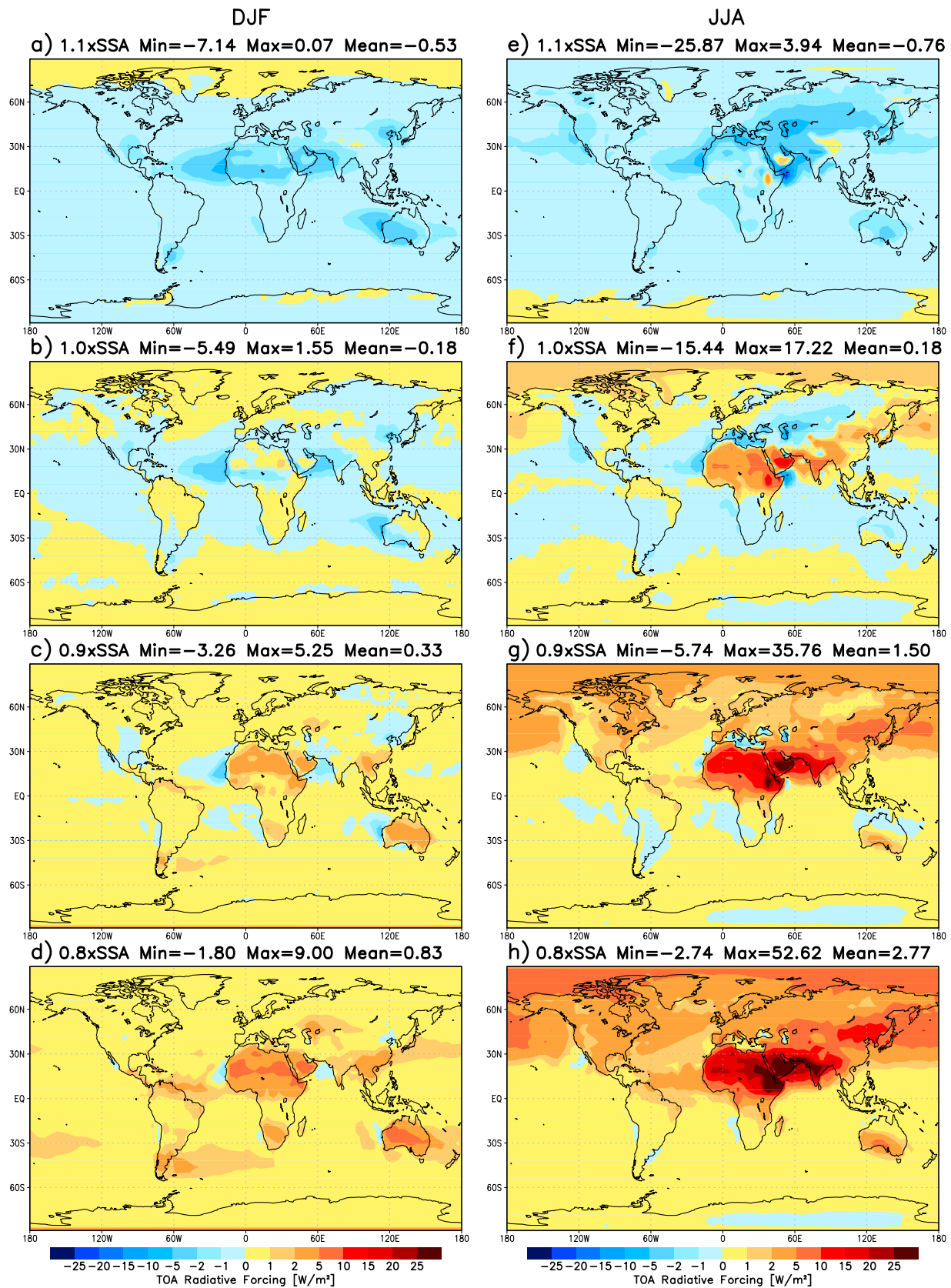


Figure 2. TOA dust radiative forcing ($W m^{-2}$) relative to the no-dust case for (a) more reflecting dust ($1.1 \times SSA$), (b) baseline dust ($1.0 \times SSA$), (c) more absorbing dust ($0.9 \times SSA$), and (d) strongly absorbing dust ($0.8 \times SSA$) for Northern Hemisphere winter (DJF). (e–h) The same as Figures 2a–2d but for summer (JJA).

Table 1. Seasonal and Annual Means of the Globally Averaged TOA Radiative Forcing for More Reflecting Dust, Baseline Dust, More Absorbing Dust, and Strongly Absorbing Dust^a

Season	1.1 × SSA	1.0 × SSA	0.9 × SSA	0.8 × SSA
DJF	−0.53	−0.18	0.33	0.83
MAM	−0.69	−0.06	0.86	1.76
JJA	−0.76	0.18	1.50	2.77
SON	−0.66	−0.14	0.62	1.37
ANN	−0.66	−0.05	0.83	1.69

^aUnit is W m^{-2} . More reflecting dust is denoted as $1.1 \times \text{SSA}$, baseline dust is denoted as $1.0 \times \text{SSA}$, more absorbing dust is denoted as $0.9 \times \text{SSA}$, and strongly absorbing dust is denoted as $0.8 \times \text{SSA}$.

cloud cover decrease with increasing radiative forcing. The sensitivity of the cloud cover response to a change in the SSA of the dust particles is largest in summer and smallest in winter. For more absorbing dust and strongly absorbing dust, the globally averaged low cloud cover change during Northern Hemisphere summer is about 0.6% and 1%, respectively, compared to $41.78\% \pm 0.03\%$ for the ensemble mean and standard deviation in the simulations without dust radiative forcing. The stronger sensitivity in summer is presumably linked to the higher dust AOD in this season. As the dust AOD increases, so does the sensitivity of the dust radiative forcing to the radiative properties and, in turn, the response of the cloud cover to the forcing.

[18] Since regional differences in the cloud cover response might be smoothed out in the global average, we also analyzed the cloud cover response combined and separately for land and sea for different ranges of the dust AOD (Figures 3b–3g). For regions with high dust AOD (seasonally averaged dust AOD ≥ 0.1), low cloud cover decreases in all seasons due to radiative forcing for more reflecting dust. The low cloud cover anomaly turns positive and increases in magnitude with increasing dust absorptivity both over land and sea, except during Northern Hemisphere winter. The sensitivity of the low cloud cover response to aerosol absorptivity is highest over land in the summer season. However, the low cloud cover response is negative with little sensitivity during Northern Hemisphere winter. Medium and high cloud cover also exhibit little sensitivity to the forcing in winter, spring, and fall. In contrast, both medium and high cloud cover increase significantly in high-dust regions with increasing radiative forcing in summer.

[19] In regions with dust AOD < 0.1 , low cloud cover increases with the magnitude of the dust radiative forcing in all seasons only over sea, whereas medium and high cloud cover decrease. Over land, low cloud cover exhibits a slight decrease or is nearly unchanged with increasing absorptivity of the dust aerosols. However, the cloud cover anomalies, averaged over all grid boxes with lower dust AOD, are small compared to regions with high dust loading. We also carried out the analysis distinguishing more classes of the dust AOD within this range ($0.1 > \text{dust AOD} \geq 0.05$, $0.05 > \text{dust AOD} \geq 0.02$, and $0.02 > \text{dust AOD}$). The results are qualitatively the same, but the magnitude of the cloud cover response decreases with decreasing dust AOD. Therefore, we considered it sufficient to distinguish only between high dust AOD and lower dust AOD in our further analysis.

[20] The ensemble mean geographical distribution of the low cloud cover response is shown in Figure 4 for the different SSA and Northern Hemisphere winter and summer.

The changes in the fractional cloud cover are displayed using contour lines. The colored shadings in Figure 4 show the probability levels with which the cloud cover changes are statistically significant, based on Student’s t test, with “negative” probabilities indicating a decrease. In winter (Figures 4a–4d), low cloud cover decreases over North Africa and the Saudi Arabian Peninsula as well as over Australia for all SSA values. These are the regions with the highest dust AOD in winter, exhibiting the negative response to dust radiative forcing with little sensitivity to its magnitude, as seen in Figure 3. However, low cloud cover increases with decreasing SSA in regions with lower or negligible dust AOD, the southern Atlantic, the southern and eastern Pacific, and the United States as well as in the area of the ITCZ from the equatorial Atlantic, over the central part of Africa to the western Indian Ocean. Note that because of the long simulations and ensemble averaging, these changes far from large dust loads are statistically significant and are the remote response to aerosol forcing.

[21] In summer (Figures 4e–4h), the largest low cloud cover increase with decreasing SSA of dust is located over northeastern Africa and the Arabian Peninsula amounting to more than 10% and about 20% for more absorbing dust and strongly absorbing dust, respectively. The area with significant low cloud cover increase extends to the west over Africa north of the equator in the area of the summer ITCZ and the northern Atlantic and to the east to India, southeastern Asia, and the northern Pacific. On the other hand, there is a significant large-scale low cloud cover decrease in an area extending from the northern part of Africa over Europe and the entire northern part of Asia. Other areas with significant low cloud cover decrease are the western part of North America and northern South America. For more reflecting dust, the cloud cover response shows a similar pattern as for more absorbing dust but with a reversed sign of the response. These changes in the low cloud cover far from the dust source regions, which are statistically significant, indicate changes in the general circulation, which are discussed in section 7.

[22] In regions with high dust AOD, positive dust radiative forcing leads to a decrease in the low cloud cover, consistent with the conventional understanding of the semi-direct effect, only in Northern Hemisphere winter. These are regions located far from tropical precipitation. In contrast, during Northern Hemisphere summer, low cloud cover increases due to dust radiative forcing by absorbing aerosols in regions with a convergent circulation such as North Africa and India. A similar tendency is found during Southern Hemisphere summer near the ITCZ over central Africa and in the South Pacific Convergence Zone (SPCZ), though. The

Table 2. Seasonal and Annual Means of the Globally Averaged Surface Radiative Forcing for More Reflecting Dust, Baseline Dust, More Absorbing Dust, and Strongly Absorbing Dust^a

Season	1.1 × SSA	1.0 × SSA	0.9 × SSA	0.8 × SSA
DJF	−0.76	−1.12	−1.63	−2.14
MAM	−1.09	−1.67	−2.49	−3.29
JJA	−1.45	−2.23	−3.30	−4.33
SON	−1.00	−1.48	−2.17	−2.85
ANN	−1.07	−1.63	−2.40	−3.16

^aUnit is W m^{-2} . More reflecting dust is denoted as $1.1 \times \text{SSA}$, baseline dust is denoted as $1.0 \times \text{SSA}$, more absorbing dust is denoted as $0.9 \times \text{SSA}$, and strongly absorbing dust is denoted as $0.8 \times \text{SSA}$.

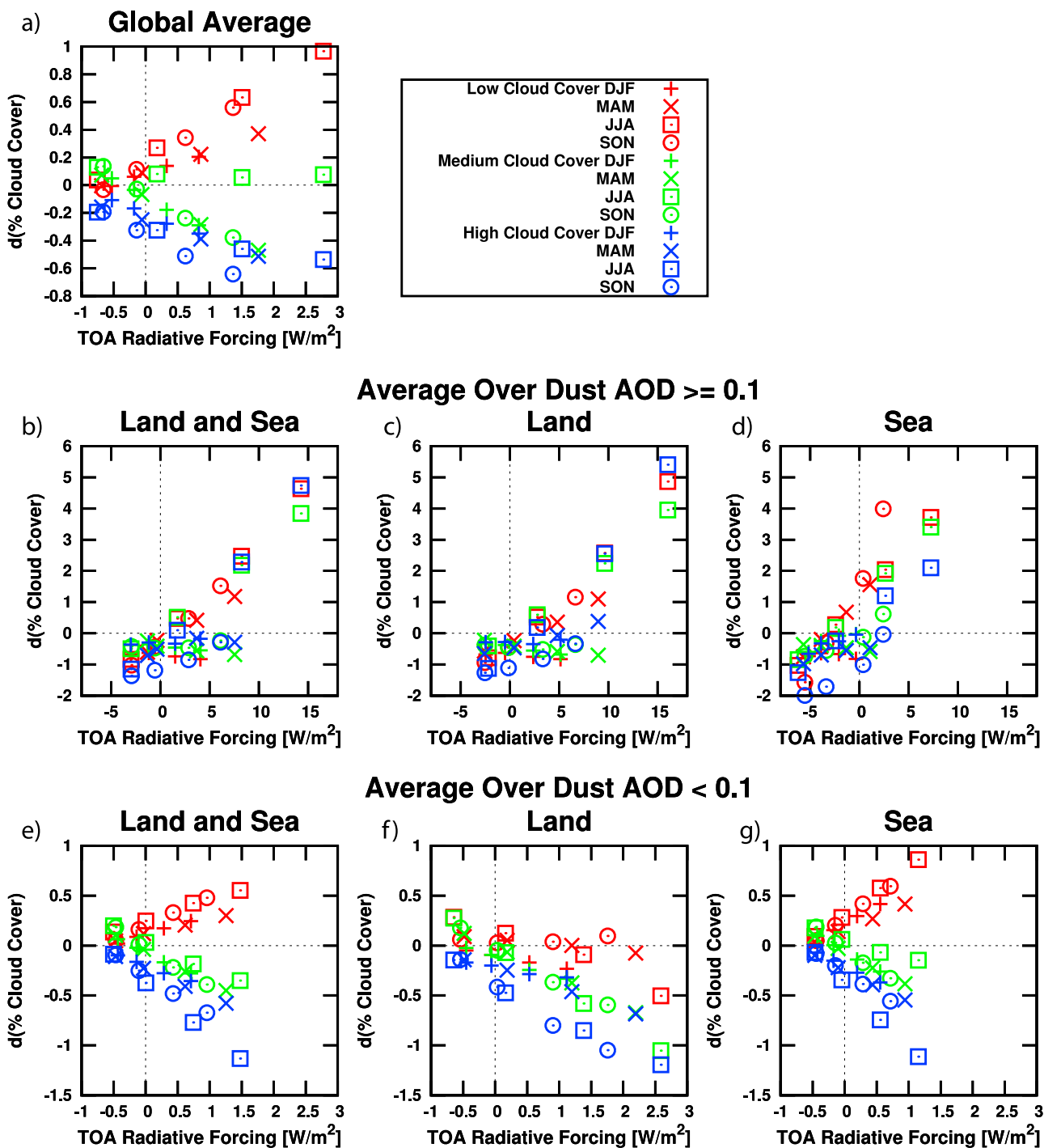


Figure 3. TOA dust radiative forcing versus change of the ensemble mean cloud cover fraction in the lower (low clouds, layers 1, 2, and 3), middle (medium clouds, layers 4 and 5), and upper troposphere (high clouds, layers 6 and 7) in the seasons. (a) Global average; average over grid boxes with dust AOD ≥ 0.1 for (b) land and sea, (c) land only, and (d) sea only; and average over grid boxes with dust AOD < 0.1 for (e) land and sea, (f) land only, and (g) sea only.

latter is located downwind of the Australian dust source region (Figure 1).

[23] The geographical distribution of the high cloud cover response is shown in Figure 5 for Northern Hemisphere winter and summer. Although high cloud cover decreases in the global average, with a stronger decrease when dust particles are made more absorbing, there are also large-scale

areas with a positive cloud cover change, particularly in the summer season of the experiments with more absorbing dust particles (Figures 5g and 5h). The strongest increase is found in an area stretching from eastern North Africa over the Saudi Arabian peninsula and South Asia to southeastern Asia. This is the same area where low cloud cover increases strongly for more absorbing dust.

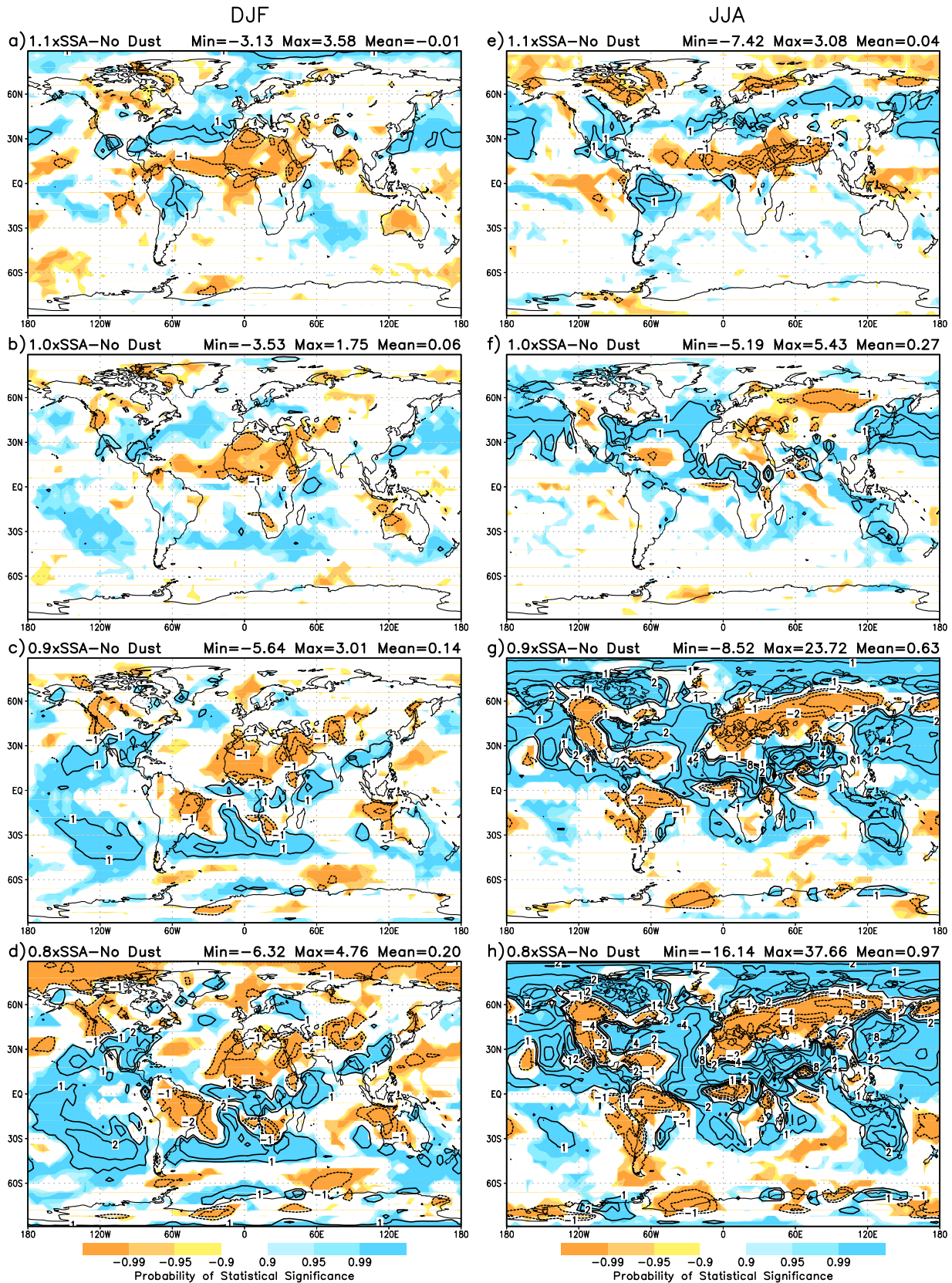


Figure 4. Response of ensemble mean low cloud cover fraction (%) (contour lines) to dust radiative forcing for (a) more reflecting dust, (b) the baseline dust, (c) more absorbing dust, and (d) strongly absorbing dust for Northern Hemisphere winter (DJF). (e–h) The same as Figures 4a–4d but for Northern Hemisphere summer (JJA). Figures 4a–4h show the probability of statistical significance of the responses for the probability levels 0.9, 0.95, and 0.99 (shading). “Negative” probability values indicate a decrease.

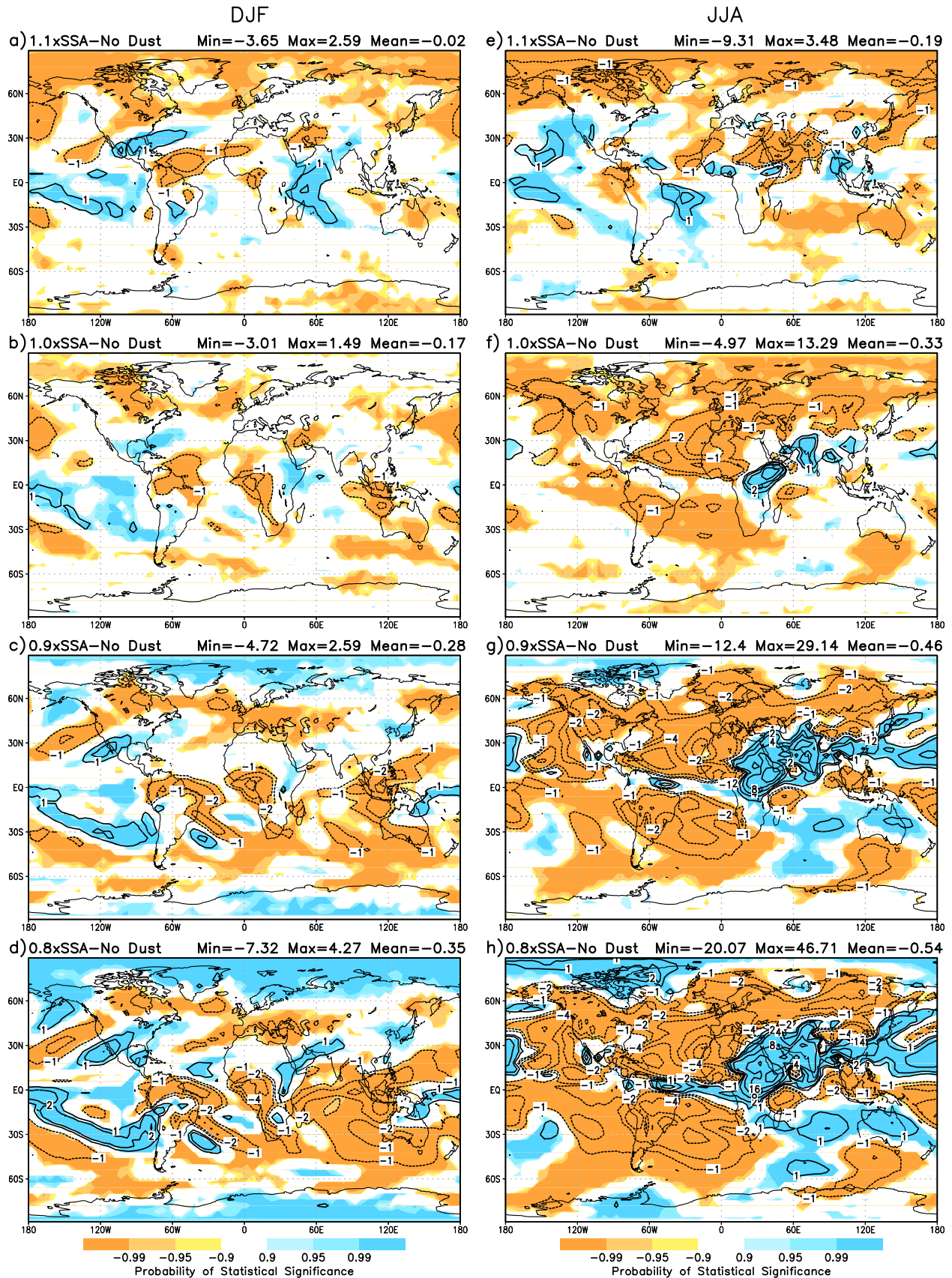


Figure 5. The same as Figure 4 but for high cloud cover fraction (%).

[24] In winter (Figures 5a–5d), high cloud cover decreases with a lower SSA in wide areas. Significantly more high cloud cover is found for more absorbing dust in the area of the SPCZ, though, and this convective region is shifted eastward by distant aerosol absorption.

5. Cloud Cover and Moisture Change

5.1. Cloud Cover and Relative Humidity

[25] Clouds are generally observed to form on scales smaller than the few hundred kilometer extent of an atmospheric GCM grid box. To represent the stratiform clouds whose anomalies are shown in Figure 3, the parameterization scheme of *Del Genio et al.* [1996] distinguishes a grid box between a cloudy part and a clear part. The water vapor tendency in the grid box determines condensation in the cloudy part and the tendency of relative humidity in the clear part. The area of the cloudy part depends on how much relative humidity in the clear part exceeds a threshold value, above which condensation occurs. Thus, although condensation takes place in nature when the water vapor pressure exceeds its saturation value, condensation in the model grid box occurs above a humidity threshold that is smaller.

[26] Cloud formation is favored in the GCM when the grid box average of specific humidity increases. Conversely, increasing temperature raises the saturation threshold of specific humidity, inhibiting cloud formation. To diagnose cloud cover changes in the model, we compute the perturbed relative humidity and the individual contributions corresponding to perturbations of temperature and moisture. Because relative humidity is not archived by the atmospheric GCM, we have to reconstruct it a posteriori using monthly averages of temperature and specific humidity. Because relative humidity depends nonlinearly on these quantities, its reconstructed monthly average is only an approximation. Moreover, cloud cover does not change linearly with relative humidity in the GCM cloud parameterization. The consistency of the cloud cover change and the perturbation to relative humidity by dust radiative forcing is one measure of whether our reconstruction and diagnosis are useful.

[27] Since the water vapor pressure is negligibly small compared to the pressure of air, we can express the relative humidity r as the ratio of the specific humidity q and the saturation specific humidity q_s ,

$$r = \frac{q}{q_s}. \quad (1)$$

[28] After applying the natural logarithm and linearizing the equation for a small perturbation to the time-averaged state of the system, we obtain an approximation for the fractional change of the relative humidity,

$$\frac{\delta r}{r} = \frac{\delta q}{q} - \frac{\delta q_s}{q_s}. \quad (2)$$

[29] When we insert the differential form of the Clausius-Clapeyron equation at constant pressure, we obtain the fractional change of relative humidity from the sum of the fractional changes of both specific humidity and temperature T ,

$$\frac{\delta r}{r} = \frac{\delta q}{q} - \frac{L_v \delta T}{R_v T^2}, \quad (3)$$

where L_v is the latent heat of water vapor and R_v is the ideal gas constant of water vapor. Since specific humidity and temperature are output as monthly averages, we use these to reconstruct approximately the fractional change of monthly average relative humidity due to dust radiative forcing.

[30] The vertical profiles of the fractional relative humidity change and the associated cloud cover response are displayed in Figure 6 for the area average over both high and lower dust AOD and in Northern Hemisphere winter and summer. In winter, within the region of high dust AOD, relative humidity decreases because of dust radiative forcing in all tropospheric layers with some sensitivity to the magnitude of the forcing. The relative humidity is much more sensitive to the forcing in summer, when changes are well correlated with the cloud cover response. Relative humidity decreases for more reflecting dust throughout the troposphere and increases for the more and the strongly absorbing dust experiments. In regions with lower dust AOD, the correlation between the relative humidity change and cloud cover response is less evident, particularly in Northern Hemisphere winter. This may indicate that reconstructing the change of relative humidity using the linearized equation (3) and monthly mean output from the model is not sufficiently accurate for lower dust AOD, where the forced changes are smaller, especially compared to unforced climate variability that is highest in winter. However, the emphasis of our analysis is on the cloud cover response in regions with high dust AOD, when our use of the linearized equation appears to be sufficient for our study.

[31] Using this linearization, we examine the relative contribution of temperature and specific humidity to the change of the reconstructed relative humidity. The increase in the temperature due to radiative forcing by absorbing aerosols has its maximum in the upper troposphere (Figure 7). Although the atmospheric heating is largest near the surface where the dust load is highest [also see *Miller et al.*, 2004, Figure 11], the warming is largest in the upper troposphere, presumably because of vertical mixing by deep convection and relaxation toward a convectively neutral lapse rate. This dynamic redistribution of heat and the maximum increase of temperature above the aerosol layer stand in contrast to the conventional description of the semidirect effect, which emphasizes the maximum temperature increase in the absorbing aerosol layer.

[32] The vertical profiles of the specific humidity and temperature terms contributing to the fractional change of relative humidity are displayed in Figure 8 for Northern Hemisphere winter and summer. The pattern of the temperature contribution to the relative humidity change is similar for high and lower dust AOD as well as for the different seasons. The magnitude of the temperature contribution, which increases with the dust AOD, is larger in Northern Hemisphere summer than in winter. For more reflecting dust, the temperature component of relative humidity increases slightly as a result of negative forcing and decreasing temperature, with little dependence on altitude. When the absorptivity of the dust particles is increased, the temperature contribution to the relative humidity becomes negative and increases in magnitude. The reduction of the relative humidity due to the temperature change by absorbing aerosols increases with altitude.

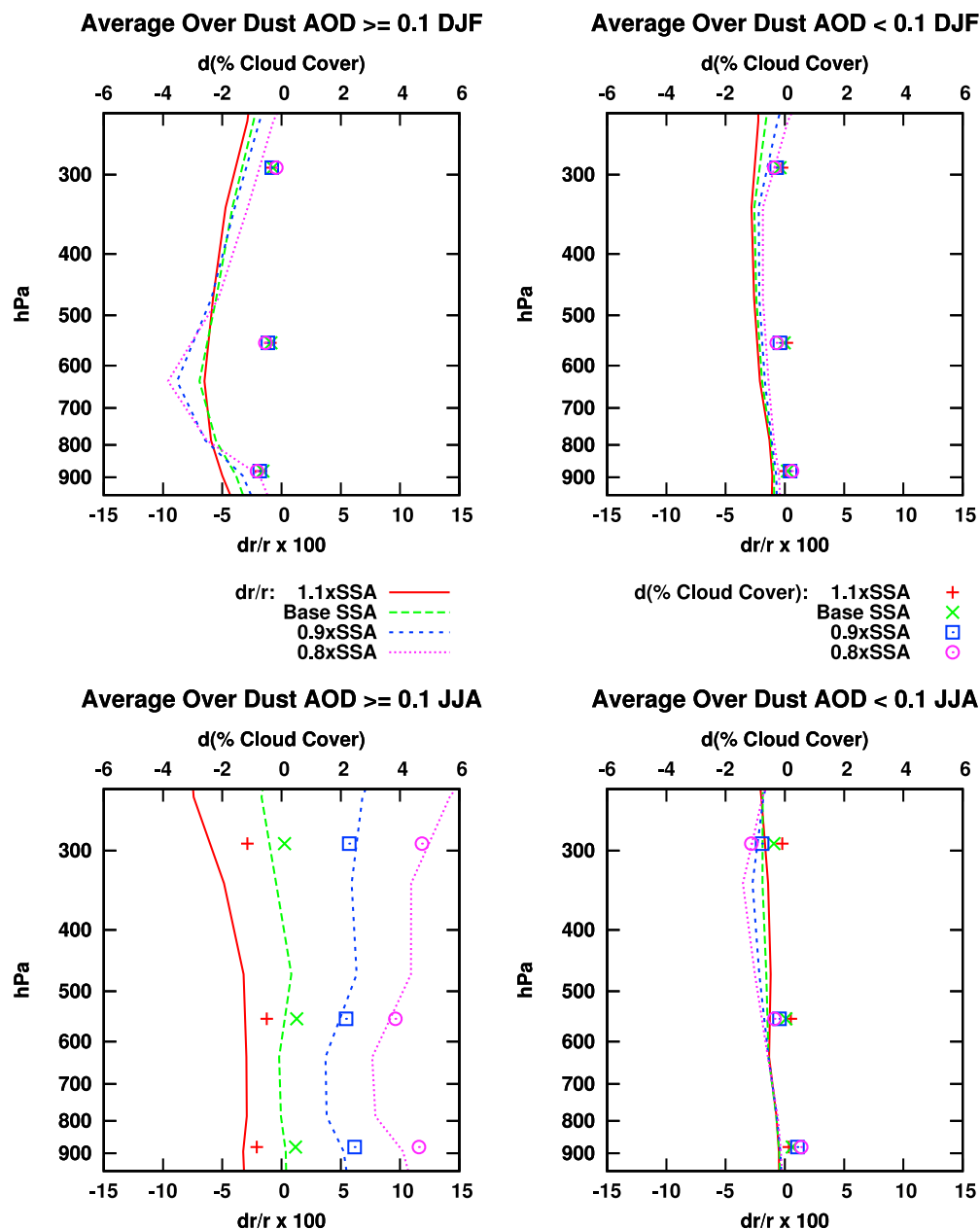


Figure 6. Vertical profiles of ensemble mean fractional change dr/r (lines) of the relative humidity r and response of the ensemble mean cloud cover fraction (symbols; difference of the percentage fractions) to dust radiative forcing for dust particles with different SSA for (left) dust AOD ≥ 0.1 and (right) dust AOD < 0.1 and Northern Hemisphere (top) winter and (bottom) summer.

[33] The contribution of specific humidity to the relative humidity change also depends upon the absorptivity of the dust particles and opposes the effect of temperature. For more reflecting dust, specific humidity decreases, lowering the relative humidity. The specific humidity change becomes less negative and turns positive (except in winter) with higher absorptivity of the dust particles. The strongest moisture increase is found in the high-dust regions in summer, whereas moisture and relative humidity decrease even for strongly absorbing dust in the high-dust regions in winter. Therefore, the net increase in relative humidity for absorbing dust in the high-dust regions in summer is due to the overwhelming effect of the increase in water vapor, which is larger than the

relative humidity decrease due to the temperature change. In contrast, in the high-dust region in winter, both the temperature and specific humidity contribute to lower relative humidity, particularly in the lower half of the troposphere. The change in cloud cover thus follows the perturbation of troposphere moisture, raising the question of by what mechanism this quantity is altered by absorbing aerosols.

5.2. Moisture Change in Lower and Upper Troposphere

[34] In the following, we relate changes in the tropospheric humidity to the TOA radiative forcing. The fractional change of the saturation specific humidity $\delta q_s/q_s$ (a sole

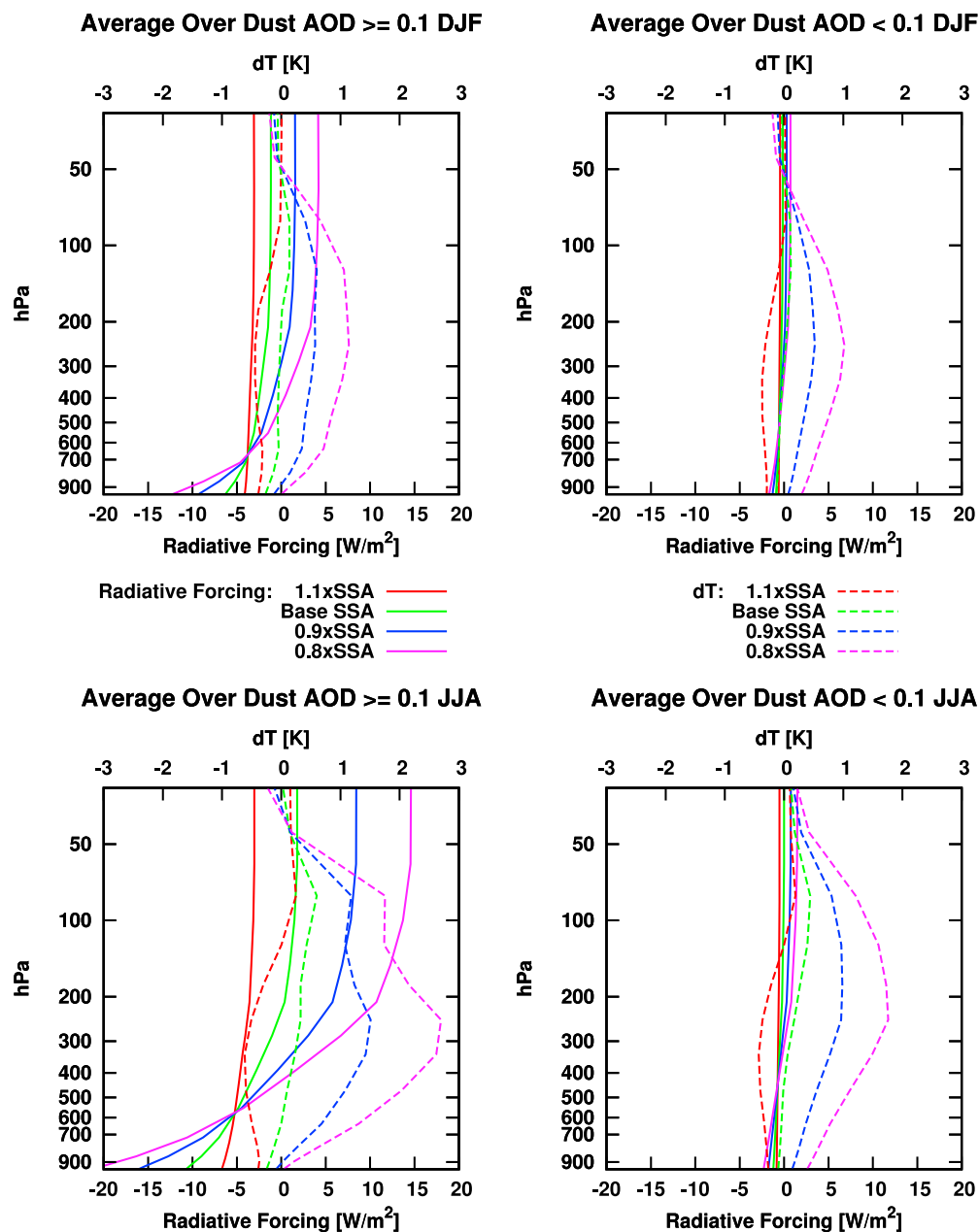


Figure 7. Vertical profiles of dust radiative forcing (W m^{-2}) (solid) and ensemble mean temperature response dT (K) (dashed) for dust particles with different SSA for (left) dust AOD ≥ 0.1 and (right) dust AOD < 0.1 and Northern Hemisphere (top) winter and (bottom) summer.

function of temperature) in the lower and upper troposphere is displayed as a function of dust radiative forcing at TOA in Figure 9. Here $\delta q_s/q_s$ was calculated as a mass-weighted average from the lowest three layers and layers six and seven, consistent with the definition of low cloud and high cloud in the model, respectively. Saturation-specific humidity increases almost linearly with the TOA radiative forcing in all seasons, although in the high-dust regions, the slope somewhat differs between the seasons, particularly in the lower troposphere. Where convection is frequent, we expect temperature and saturation-specific humidity in the lower troposphere to be closely linked to the TOA radiative forcing, since the temperature profile in the whole column is linked by convective mixing to the temperature in the upper tropo-

sphere, where emission of long-wave radiation to outer space adjusts to the forcing [Cess *et al.*, 1985; Miller and Tegen, 1998]. We also find that the sensitivity of the fractional change of the saturation specific humidity to the TOA radiative forcing is much larger in the upper troposphere than in the lower troposphere both for high- and low-dust regions, since the sensitivity of the temperature response to the radiative forcing is largest in upper tropospheric layers.

[35] It follows from equation (2) that the increase in the saturation-specific humidity with increasing dust radiative forcing implies lower relative humidity and less cloud cover if the specific humidity itself does not change. On the other hand, in order to have a fractional increase in the relative humidity with increasing forcing, the fractional increase in

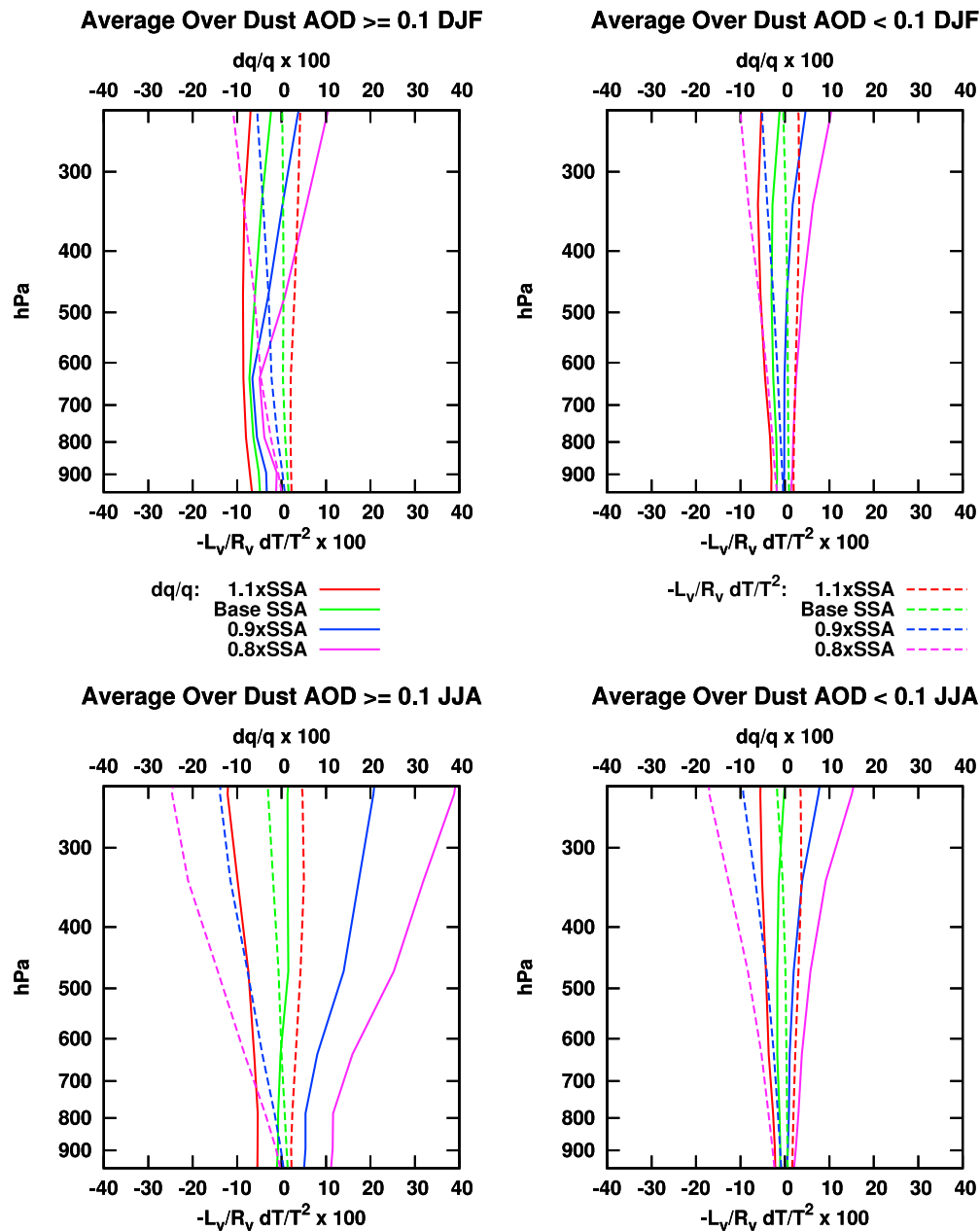


Figure 8. Ensemble mean vertical profiles of the contributions of the specific humidity change dq/q (solid) and the temperature change $-[(L_v/R_v)(dT/T^2)]$ (dashed) to the fractional relative humidity change due to dust radiative forcing for dust particles with different SSA for (left) dust AOD ≥ 0.1 and (right) dust AOD < 0.1 and Northern Hemisphere (top) winter and (bottom) summer.

the specific humidity must be larger than the increase in the saturation-specific humidity.

[36] The fractional change of specific humidity versus the fractional change of saturation-specific humidity is displayed in Figure 10 for the lower and upper troposphere and for high and lower dust AOD regions. Both variables were calculated as mass-weighted averages from the same layers as before. There is an almost linear relationship between the variables both for high dust AOD and lower dust AOD regions in all seasons. The diagonal line in each plot shows where $\delta q/q$ equals $\delta q_s/q_s$ and relative humidity is unchanged (subject to the approximation of our recon-

struction). For the lower troposphere, $\delta q/q$ clearly exceeds $\delta q_s/q_s$ for all seasons but winter given sufficient absorption. The relative magnitude of $\delta q/q$ and $\delta q_s/q_s$ for each season is roughly consistent with the sensitivity of cloud cover to TOA radiative forcing in Figure 3, showing the correspondence between relative humidity and cloud cover changes. Considering the nonlinear relationship between relative humidity and cloud cover in the model, increases in cloud cover are only approximately given by where the anomalous relative humidity is greater than zero.

[37] For lower dust AOD, the fractional specific humidity change is generally comparable with the change of the sat-

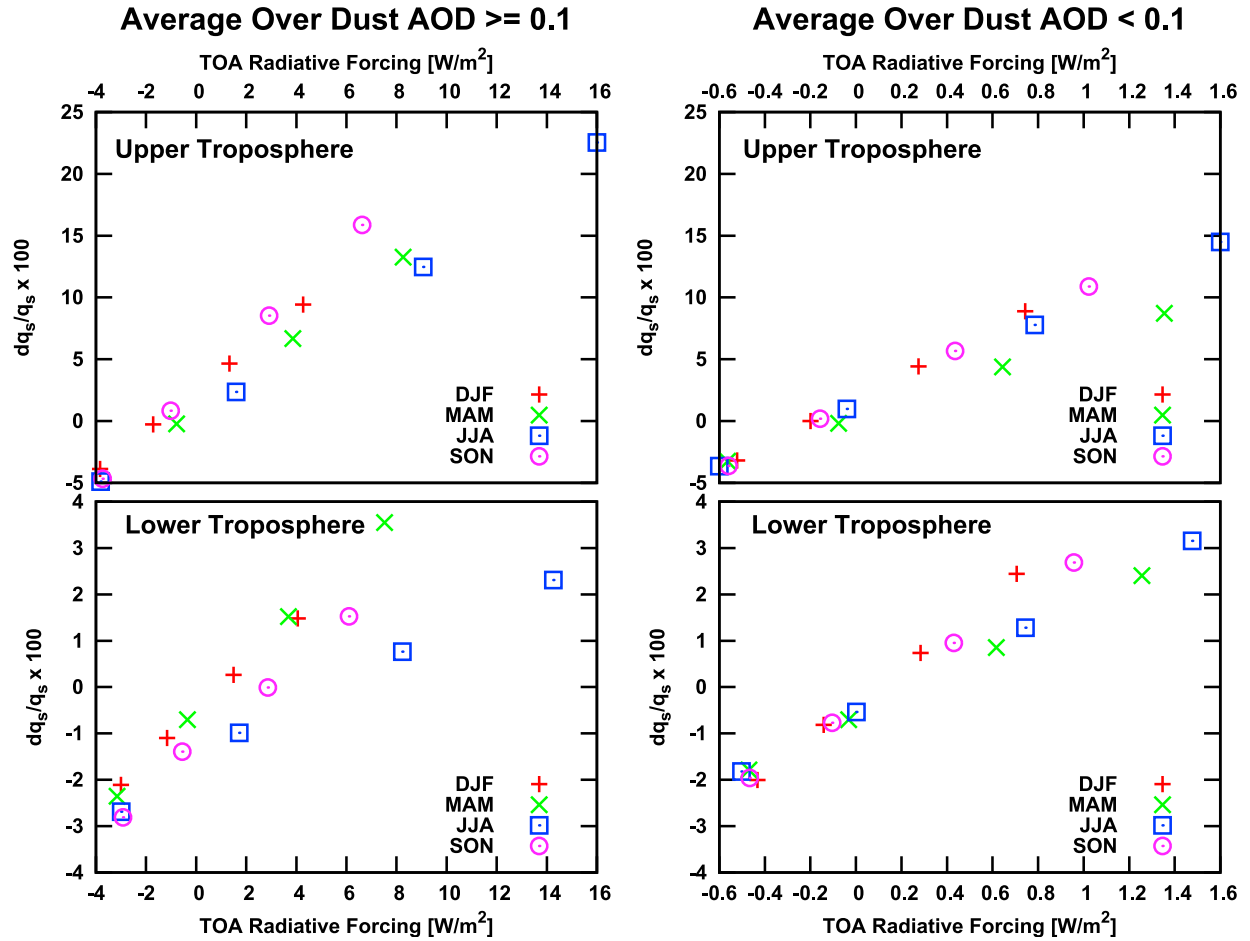


Figure 9. TOA dust radiative forcing versus ensemble mean of fractional change of saturation specific humidity dq_s/q_s (top) in the upper troposphere and (bottom) in the lower troposphere and for (left) dust AOD ≥ 0.1 and (right) dust AOD < 0.1 in the seasons.

uration specific humidity. As we pointed out in section 5.1, the correlation of the fractional relative humidity change to the cloud cover change is less evident here.

6. Evaporation, Precipitation, and Moisture Flux Change

[38] In section 5, we established that the increased low cloud cover for absorbing dust aerosols in the high-dust regions in Northern Hemisphere spring, summer, and fall is due to an increase in the specific humidity in the lower troposphere, leading to higher relative humidity, counteracting the warming effect of the absorbing aerosols. In contrast, in winter (Figure 8, top left), specific humidity decreases in the lower troposphere in the regions with dust AOD ≥ 0.1 with only a slight sensitivity to the absorptivity of the dust particles. Thus, both the temperature increase and the specific humidity decrease contribute to a lower relative humidity leading to less low cloud cover for absorbing dust aerosols, consistent with the conventional description of the semidirect effect. Now we consider the balance of specific humidity to determine the source of the additional water vapor for spring, summer, and fall.

[39] The water vapor balance has been analyzed in the previous literature [e.g., Yanai *et al.*, 1973; Sundqvist *et al.*,

1989; Trenberth and Guillemot, 1995]. We can write the vertically integrated balance of specific humidity in the atmospheric column for the equilibrium state forced by soil dust aerosols,

$$-\nabla \cdot \mathbf{M}_q = P - E, \quad (4)$$

where \mathbf{M}_q is the horizontal flux of specific humidity integrated over the atmospheric column, E is evaporation of water vapor from the underlying surface, and P is column precipitation.

[40] For the difference of each equilibrium component compared to the control ensemble without dust radiative forcing, we write

$$\delta(-\nabla \cdot \mathbf{M}_q) = \delta P - \delta E. \quad (5)$$

[41] A positive change of convergence of the specific humidity flux $-\nabla \cdot \mathbf{M}_q$ equals the change of the difference between precipitation and evaporation. In Figure 11, we display the specific humidity change in the lower troposphere (implicitly a function of the forcing) versus evaporation, precipitation, and their difference.

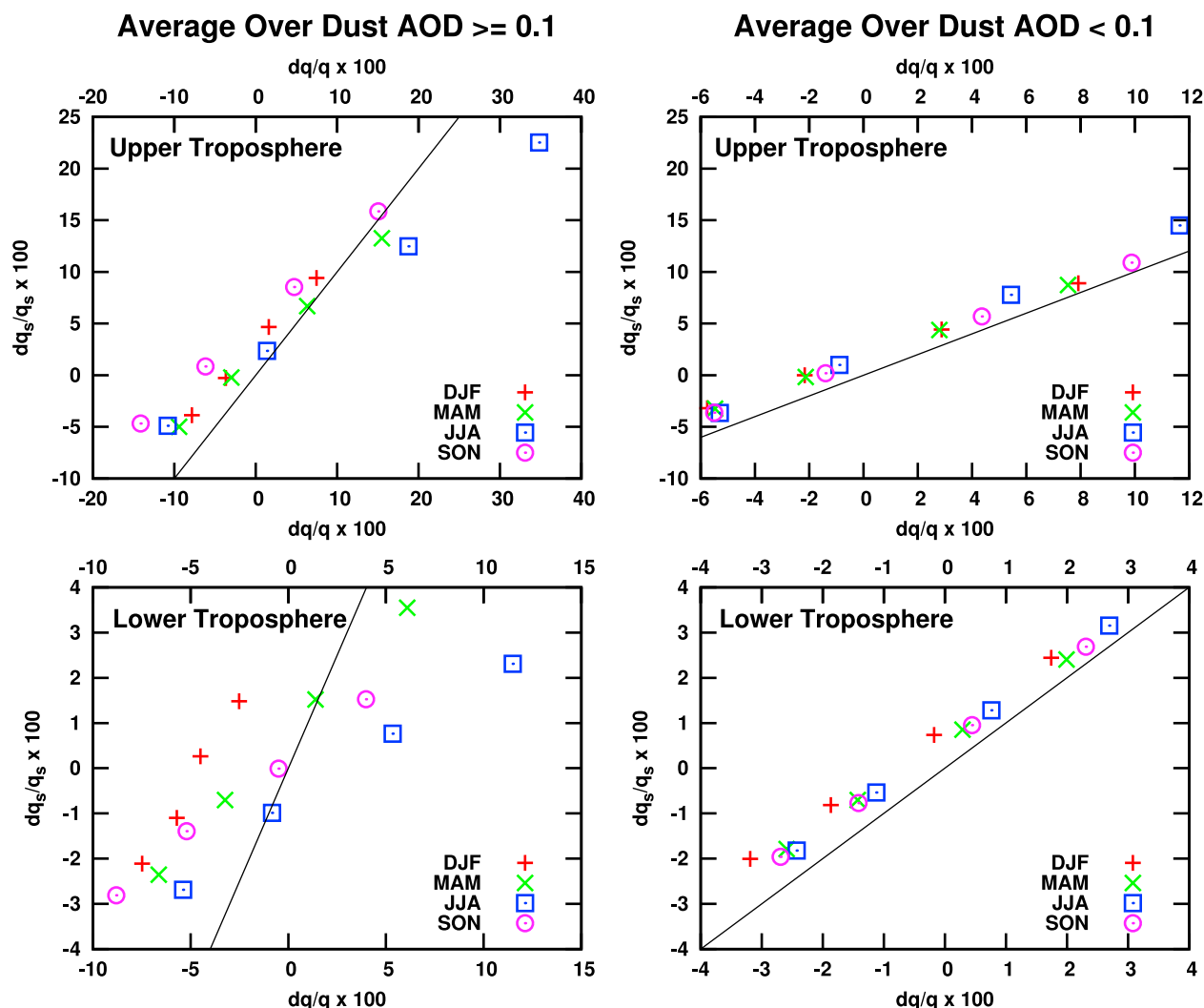


Figure 10. Ensemble mean of the fractional specific humidity change dq/q versus ensemble mean of the fractional saturation specific humidity change dq_s/q_s (top) in the upper troposphere and (bottom) in the lower troposphere for (left) dust AOD ≥ 0.1 and (right) dust AOD < 0.1 in the seasons. The diagonal lines mark where $(dq_s/dq)(q/q_s) = 1$.

[42] Evaporation is reduced by dust radiative forcing in the regions with high dust AOD in all seasons, even though the specific humidity increases for more absorbing dust in Northern Hemisphere spring, summer, and fall. The evaporation decrease is largest in summer. The evaporation response becomes less negative with increasing specific humidity and more absorbing dust, though, especially in fall and spring. In contrast, in winter, the evaporation decrease becomes larger with increasing atmospheric moisture and more absorbing dust.

[43] The relation between evaporation and dust forcing becomes more evident if we analyze the evaporation response for land and sea separately (Figure 12). Over the oceans, where there is an unlimited supply of moisture, evaporation decreases with more negative surface forcing (corresponding to increasing absorptivity of the dust aerosols) in the high-dust regions in all seasons. In contrast to the oceans, evaporation increases with more negative surface forcing in the high-dust regions over land. The evaporation response scales with the change in precipitation over land, since moisture

available for evaporation, which is scarce in arid land areas, depends in part on the supply from precipitation. The negative surface forcing over land is mainly compensated by a decrease both in the net thermal radiation and the sensible heat flux from the surface to the atmosphere (not shown). Thus, the notion that the latent heat flux decreases with increasingly negative surface radiative forcing is true in the high-dust regions only over the oceans in our simulations, as also found by *Miller et al.* [2004].

[44] Precipitation and specific humidity in the lower troposphere are strongly correlated in the high dust AOD regions in spring, summer, and fall (Figure 11). For more reflecting dust, precipitation decreases, but it turns positive and increases with increasing specific humidity, i.e., with increasing absorptivity of the dust particles. The precipitation increase for absorbing dust is largest in summer, when the dust AOD is highest and dust radiative forcing is strongest. Land areas provide the main contribution to the precipitation increase (Figure 12). In contrast, in winter, precipitation generally decreases in the high dust AOD

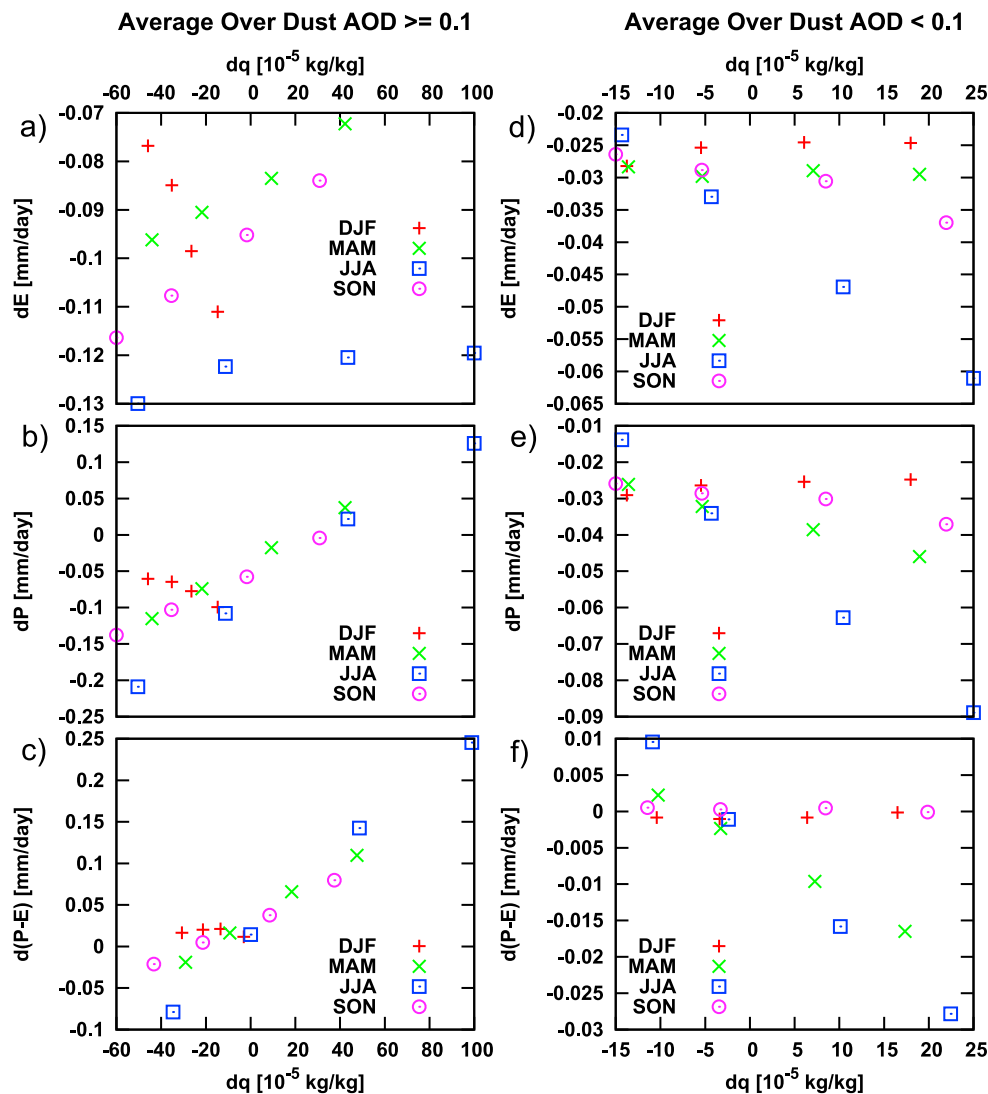


Figure 11. Change of ensemble mean specific humidity dq in lower troposphere versus change of the ensemble mean evaporation dE , precipitation dP , and difference between evaporation and precipitation $d(P - E)$ for (a–c) dust AOD ≥ 0.1 and (d–f) dust AOD < 0.1 in the seasons.

regions with little sensitivity to the lower troposphere specific humidity change.

[45] Reduced evaporation and increased precipitation mean that an increased specific humidity and cloud cover must be due to an increased convergence of water vapor according to equation (5). The difference between precipitation and evaporation is shown in Figures 11c and 13 (left). The correlation between specific humidity in the lower troposphere and precipitation–evaporation difference during all seasons, except during Northern Hemisphere winter, indicates a transition from increased water vapor divergence for more reflecting dust to an increased convergence for more absorbing dust. We conclude that forcing by absorbing dust drives circulation changes in spring, summer, and fall that increase the horizontal influx of water vapor mass, which contributes to increased low-level specific humidity and cloud cover in the high dust AOD regions.

[46] The geographical distribution of both the changes in the vertically integrated water vapor mass flux and precipitation minus evaporation confirms that in the case of

absorbing dust there is an increased moisture convergence in the high dust AOD regions in Northern Hemisphere summer, particularly over northeastern Africa, the Saudi Arabian Peninsula, and India (Figure 14). Note that the water vapor flux is already convergent in these regions in the no-dust control ensemble. For more reflecting dust, the picture is reversed, and the water vapor flux becomes less convergent in the regions of high dust AOD. These changes are consistent with the cloud cover changes both for reflecting dust and absorbing dust.

[47] In contrast, in Northern Hemisphere winter (Figure 15), the water vapor flux in the no-dust control ensemble is convergent over equatorial Africa and south, when the ITCZ is shifted southward. The major dust source regions in North Africa and the Saudi Arabian Peninsula and the dust plume over the North Atlantic are located in a subsidence branch of the Hadley–Walker circulation system. Reflecting dust decreases the moisture divergence in these regions somewhat, whereas absorbing dust increases it somewhat over land. This agrees with the slightly larger reduction in

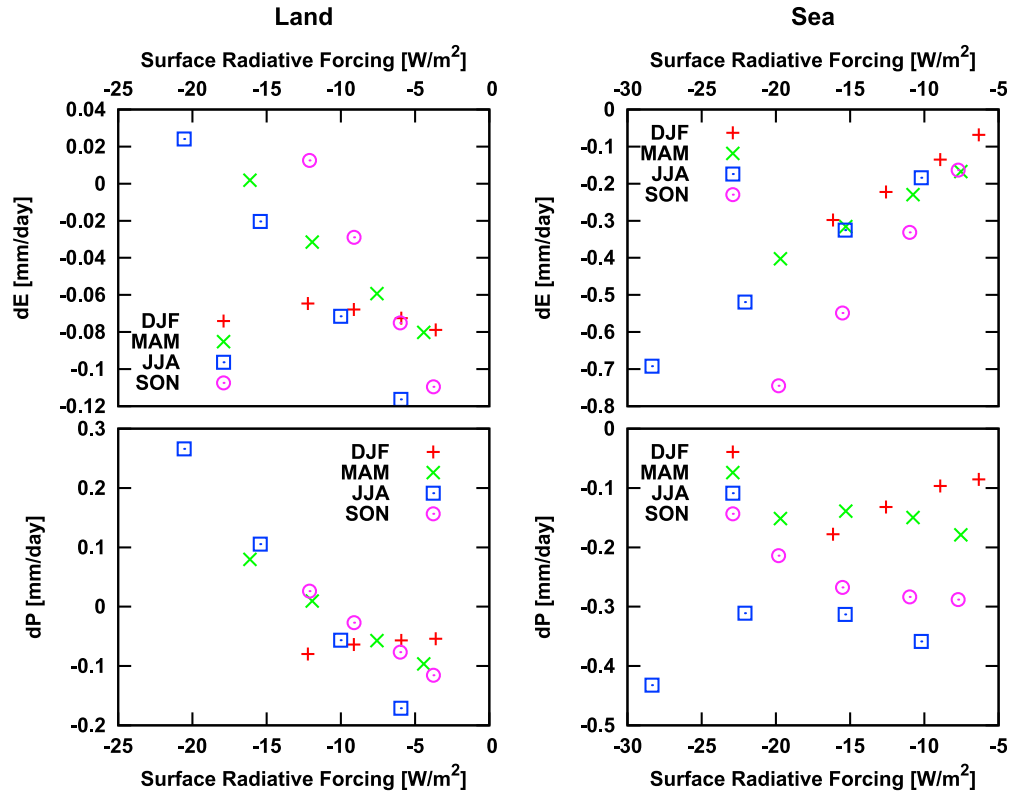


Figure 12. Surface dust radiative forcing versus change of ensemble mean evaporation dE and precipitation dP for dust $AOD \geq 0.1$ over (left) land and (right) sea in the seasons.

low cloud cover in high-dust regions in winter (Figure 3) for absorbing dust, consistent with the conventional understanding of the semidirect effect of absorbing aerosols.

[48] Note that there is an increased water vapor flux into the SPCZ, particularly for strongly absorbing dust in northern winter, which is also consistent with the cloud cover changes we observed in our simulations. This region is affected by the dust plume from Australia, which has its maximum in Southern Hemisphere summer. Radiative forcing by absorbing aerosols has an effect on the circulation in the southern Pacific that is similar to the effect of absorbing

aerosols on cloud cover and circulation in the high dust AOD regions of the Northern Hemisphere during local summer.

[49] Over regions with lower dust AOD, both evaporation and precipitation generally decrease as a result of dust radiative forcing, although the response is sensitive to the forcing in Northern Hemisphere summer only. In this season, specific humidity is anticorrelated with both variables. The column moisture divergence increases with both low-level specific humidity (Figure 11f) and low cloud cover (Figure 13, right) during spring and summer. That is, mois-

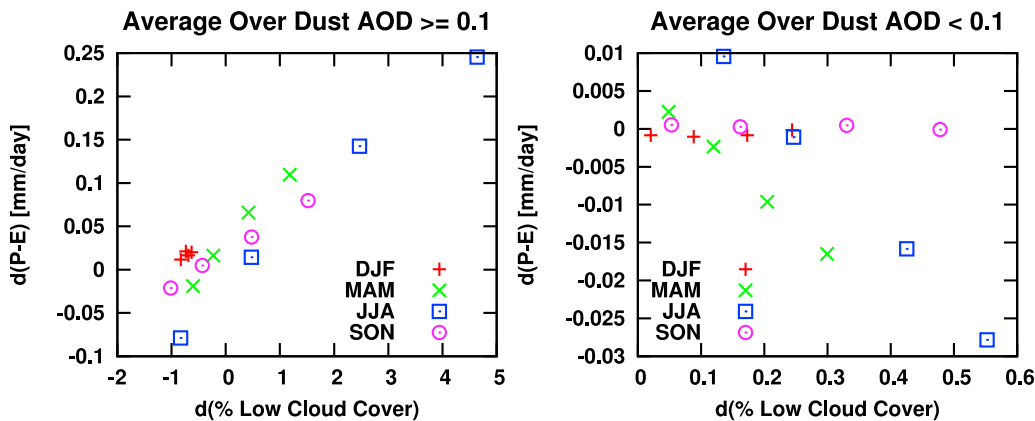


Figure 13. Change of the ensemble mean low cloud cover fraction versus change of the difference between the ensemble means of precipitation and evaporation $d(P - E)$ for (left) dust $AOD \geq 0.1$ and (right) dust $AOD < 0.1$ in the seasons.

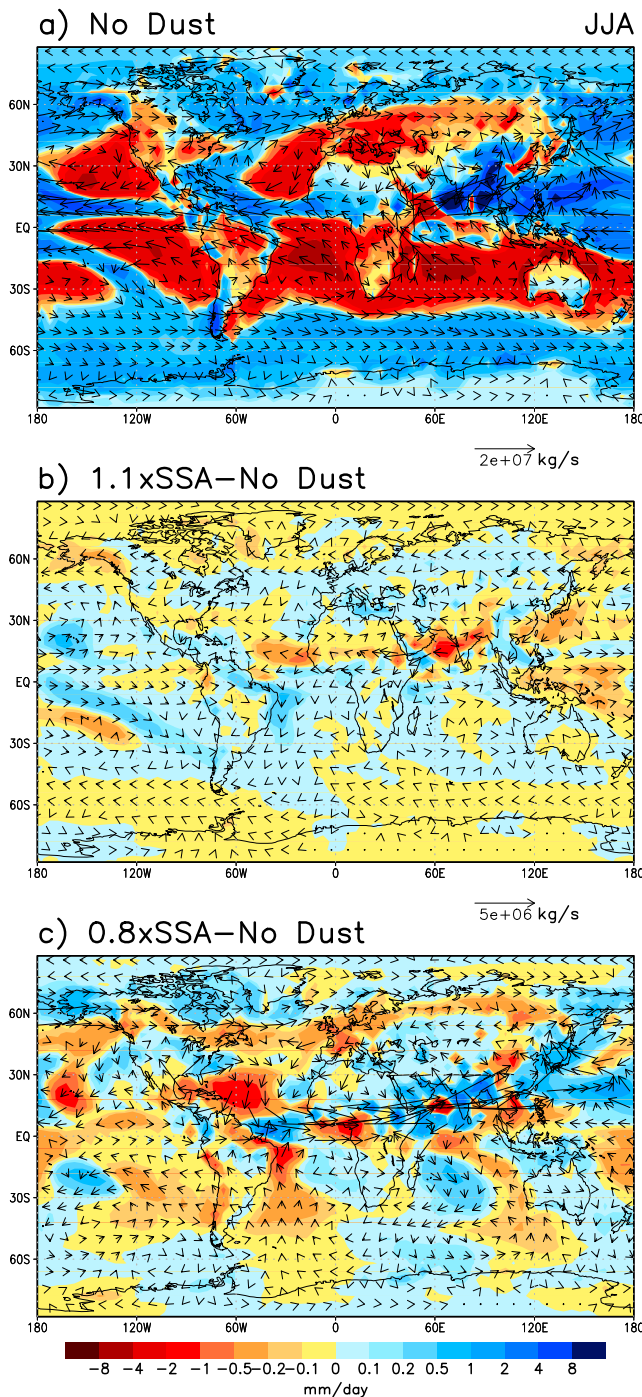


Figure 14. Ensemble means of precipitation minus evaporation (mm d^{-1}) (shaded) and mass flux of water vapor (kg s^{-1}) (vector field) for (a) the no-dust case and responses for (b) more reflecting dust and (c) strongly absorbing dust in Northern Hemisphere summer (JJA).

ture is exported to high-dust regions. When evaporation is decreased and moisture divergence over the whole atmospheric column is increased, it is possible that the larger moisture content in the lower troposphere compared to the no-dust control simulations is a result of weaker conversion of water vapor to liquid water in the lower troposphere; this is

consistent with the reduction of the precipitation rate with increasing absorptivity of the dust particles.

7. Link to Changes in the General Circulation

[50] To illustrate the circulation changes induced by dust radiative forcing in more detail, we display in Figure 16 the zonal average centered over the western Indian Ocean between 20°E and 85°E of the vertical velocity and other

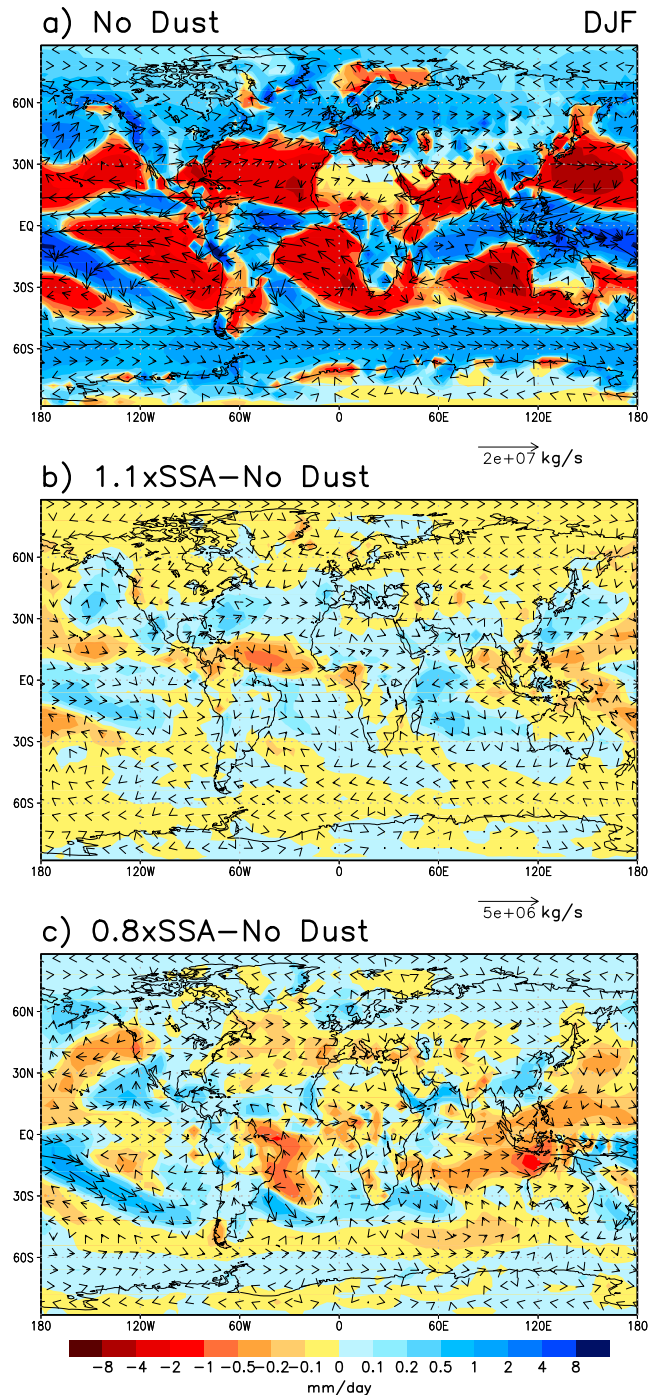


Figure 15. The same as Figure 14 but in Northern Hemisphere winter (DJF).

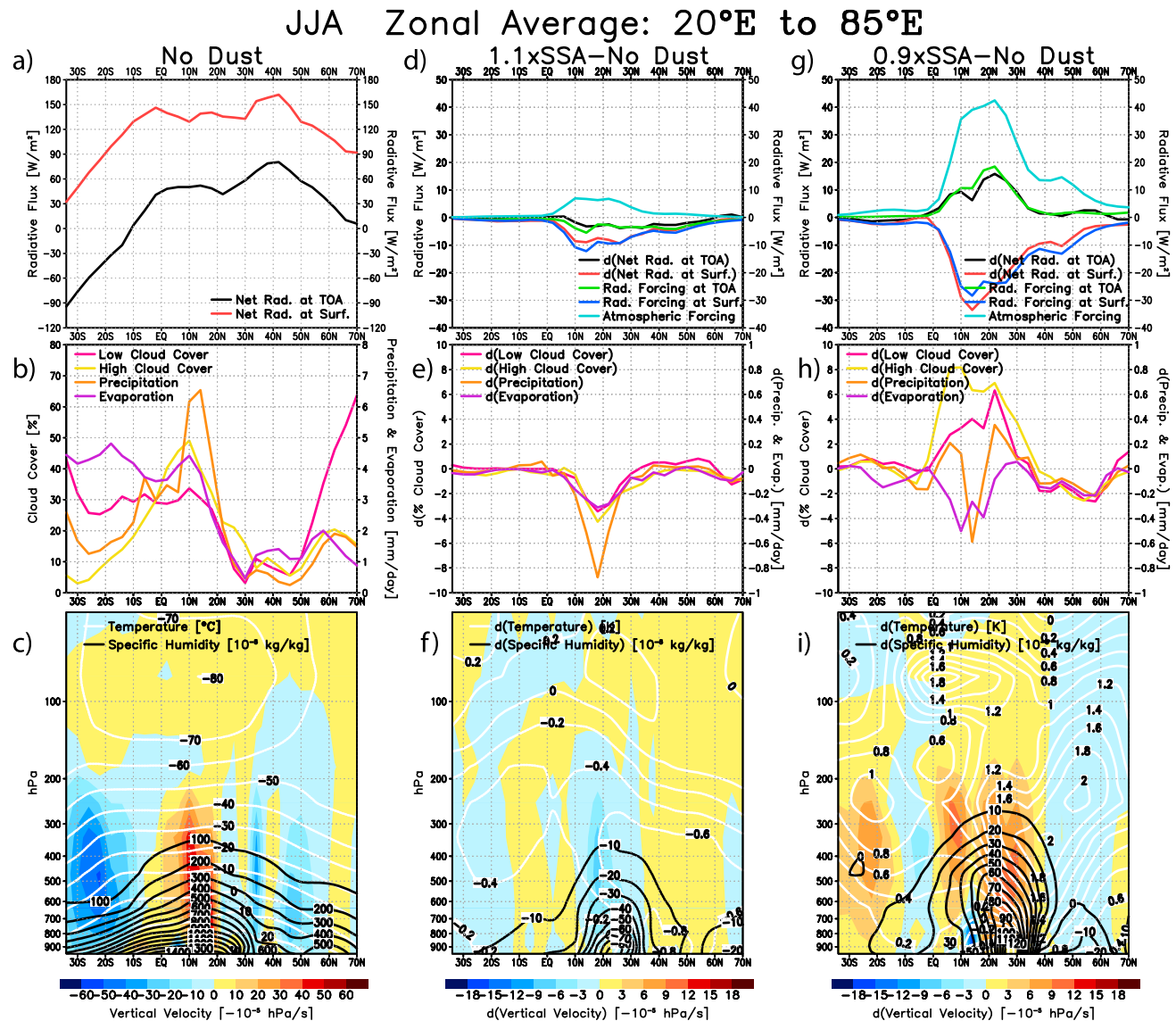


Figure 16. Ensemble mean zonal averages between 20°E and 85°E in Northern Hemisphere summer (JJA). (a–c) Reference values in no-dust case, (d–f) response for more reflecting dust, and (g–i) response for more absorbing dust. Figures 16a, 16d, and 16g show net radiative flux (W m^{-2}) at TOA and at surface as well as dust radiative forcing (W m^{-2}) at TOA and at surface and atmospheric dust radiative forcing (W m^{-2}); Figures 16b, 16e, and 16h show low cloud cover (%), high cloud cover (%), precipitation (mm d^{-1}), and evaporation (mm d^{-1}); and Figures 16c, 16f, and 16i show vertical velocity ($-10^{-5} \text{ hPa s}^{-1}$), temperature ($^{\circ}\text{C}$ or K), and specific humidity ($10^{-5} \text{ kg kg}^{-1}$).

variables for the no-dust ensemble mean and their changes for more reflecting dust and more absorbing dust during Northern Hemisphere summer. This zonal average includes the area with maximum dust radiative forcing over northeastern Africa, the Arabian Peninsula, and India. The circulation in the no-dust ensemble (Figures 16a–16c) shows rising air with maximum specific humidity and precipitation between 10°N and 20°N. The latitude dependence of high cloud cover is similar to the one of precipitation. Subsidence of air with minimum cloud cover and precipitation is found in the latitudes north and south of the convergence zone.

[51] Dust radiative forcing has its maximum at about 20°N. For more absorbing dust, the maximal atmospheric

forcing, which equals the difference between TOA radiative forcing and surface radiative forcing, zonally averaged over the sector, amounts to about 40 W m^{-2} (Figure 16g). The convergence zone and the area with elevated heating by dust overlap to a large degree. The radiative forcing by absorbing dust broadens the region of low-level convergence and rising air, leading to a northward extension of the convergence zone (Figure 16i). Moisture increases in higher tropospheric layers as a result of increased convergence. The increases in high and low cloud cover as well as precipitation (Figure 16h) are consistent with the changes in humidity. The temperature increase is maximal in the middle and upper tropospheric layers of the Northern Hemisphere. In turn, convergence of air is reduced between

DJF Zonal Average: 20°E to 60°E

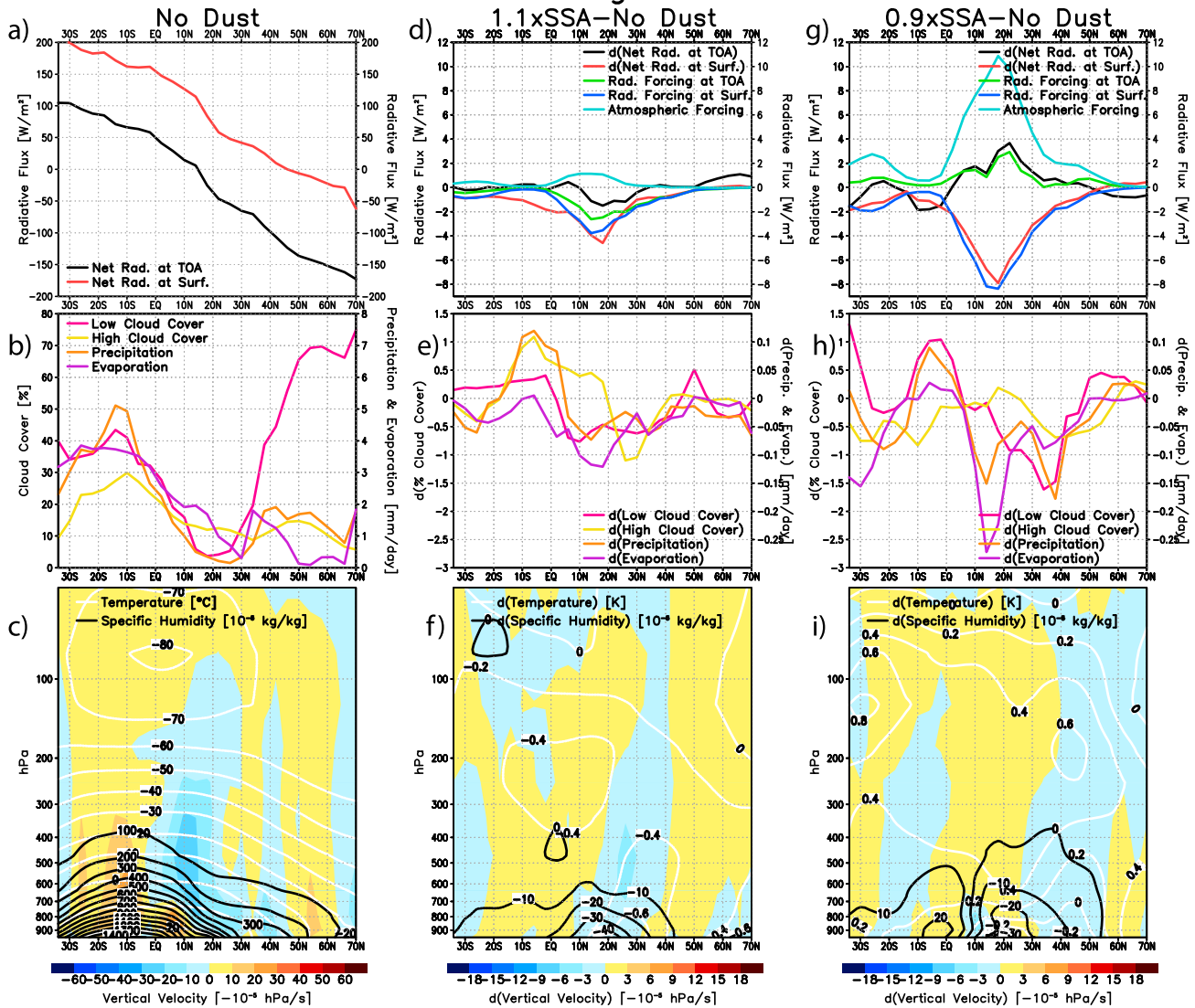


Figure 17. The same as in Figure 16 but between 20°E and 60°E in Northern Hemisphere winter (DJF).

10°N and 20°N, where rainfall is largest in the absence of dust, and subsidence of air is enhanced between 40°N and 60°N. Moisture decreases in the subsidence region only near the surface due to decreased evaporation, which is consistent with the decrease in low cloud cover in this region. Moisture increases in the higher tropospheric layers in the subsidence region, partly because of export from the convecting regions, although the increase is much smaller than in the convergence zone. High cloud cover shows a decrease despite the moisture increase, since the warming of the upper troposphere raises the saturation specific humidity, overwhelming the moisture effect on relative humidity as established in section 5.

[52] The radiative forcing due to reflecting dust (Figure 16d) has the opposite effect on the circulation (Figure 16f) compared to absorbing dust. Dust forcing in the convergence zone counteracts the upward movement of air. The moisture decrease is largest at the latitude of the maximal convergence decrease. High and low cloud cover

and precipitation are decreased accordingly. In turn, subsidence is weaker between 40°N and 60°N.

[53] The Hadley circulation is strengthened even more for strongly absorbing dust (not shown), whereas the changes in the baseline ensemble (not shown) are small, exhibiting a transition state between the response for more absorbing dust and the response with opposite sign for more reflecting dust.

[54] For Northern Hemisphere winter (Figure 17), we calculated the zonal averages of the same variables as for summer but between 20°E and 60°E. This sector includes the area of maximal dust radiative forcing over northeastern Africa and the Saudi Arabian Peninsula. The African convergence zone with maximum moisture and local maxima of high and low cloud cover as well as precipitation is located around 15°S in the no-dust ensemble (Figures 17a–17c).

[55] Dust radiative forcing in the other ensembles (Figures 17d and 17g) is maximal in the area of subsi-

dence over North Africa in this season. The atmospheric forcing by absorbing dust counteracts the subsidence (Figure 17i), whereas the convergence of air south of the equator is strengthened in its northern part, between 0° and 10°S , and weakened at around 20°S . This shift is also expressed in the precipitation response. Although moisture is increased near the surface south of the equator, the additional moisture in the area with increased convergence is mainly redistributed into tropospheric layers above in the Southern Hemisphere, whereas the moisture change in the lower troposphere in the subsidence area of northern Africa is dominated by the decrease in the evaporation due to the strong negative surface forcing. Therefore, low cloud cover decreases for more absorbing dust in the high-dust region of eastern North Africa and the Arabian Peninsula in Northern Hemisphere winter.

[56] For more reflecting dust (Figures 17d–17f), the circulation response to the radiative forcing has a sign that is opposite to the response to the forcing by absorbing dust. Subsidence over North Africa is strengthened. The atmosphere becomes cooler and drier. The moisture decrease is maximal near the surface where the evaporation decrease is maximal and the surface radiative forcing most negative, which is consistent with the low cloud cover decrease in this region.

[57] The effect of counteracting the subsidence in the region with dust radiative forcing during Northern Hemisphere winter is even stronger for strongly absorbing dust (not shown). The response in the baseline ensemble (not shown) is small, expressing a transitional state between the responses for more absorbing dust and more reflecting dust again.

[58] In summary, atmospheric heating increases with the TOA dust radiative forcing. When the forcing and a convergence zone are geographically close in our simulations, convergence is strengthened and the rise of air and the transport of moisture in upper tropospheric layers are increased, particularly in the hemisphere in which the convergence zone is located. In turn, subsidence is enhanced in the surrounding subsidence regions. In contrast, radiative forcing in a convergence zone by strongly reflecting dust acts toward a decrease of convergence and the upward transport of air and moisture in this region. Subsidence in the regions around the convergence zone is weakened. The response to both of these forcings is similar to that described by *Chou et al.* [2005].

[59] When the radiative forcing by absorbing dust is located in a subsidence region, the radiative heating counteracts the subsidence and weakens the circulation from the convergence zone to the subsidence region, whereas in contrast, strongly reflecting dust in a subsidence region strengthens the subsidence.

8. Summary and Conclusions

[60] We have reexamined the semidirect effect on cloud cover due to radiative forcing by tropospheric aerosols and the role of the hydrological response to changes involving the atmospheric circulation. We carried out ensemble simulations with the GISS general circulation model. No dust radiative forcing was prescribed in one ensemble of the simulations. Four additional ensembles were carried out with a

prescribed dust distribution based upon particles with a different single-scattering albedo.

[61] According to the conventional description of the semidirect effect, tropospheric aerosols that absorb radiation decrease relative humidity and cloud cover. Here we have presented a counterexample. In our simulations, low cloud cover increases due to radiative forcing by absorbing aerosols in high-dust AOD regions (dust AOD ≥ 0.1) during Northern Hemisphere spring, summer, and fall and in low-dust AOD regions over sea during all seasons. The strongest increase in cloud cover due to absorbing aerosols was found in high-dust AOD regions in Northern Hemisphere summer. We observed a decrease in low cloud cover in high-dust AOD regions only in winter. The cloud changes in our simulations are due only to the radiative effect of dust aerosols, since microphysical effects of dust aerosols acting as cloud droplet nuclei were not included.

[62] For absorbing dust, the increase of specific humidity in the lower troposphere overwhelms the warming effect of the absorbing aerosols on relative humidity in high-dust regions (except in Northern Hemisphere winter) and in low-dust regions over the oceans, leading to an increase in low cloud cover. In some regions where an enhanced dust radiative forcing and moisture convergence overlap, the same effect can be observed even in the middle and high troposphere, increasing cloud cover in these layers. From an analysis of the water vapor balance, we concluded that an increased horizontal influx of water vapor from surrounding areas contributes to the increase in the specific humidity in high-dust AOD regions during spring, summer, and fall.

[63] In our experiments, radiative forcing by soil dust aerosols has a significant effect on climate, not just in regions with high dust AOD but also in remote regions via large-scale circulation changes. The magnitude and even the sign of these large-scale changes depend on the radiative properties of the dust particles. For instance, low cloud cover significantly decreases and increases for more absorbing dust and more reflecting dust, respectively, over the whole region stretching from Europe to East Asia in Northern Hemisphere summer as well as over northern South America in the same season. This raises the possibility that low cloud cover changes in such regions interpreted as the effect of local forcing could actually result from large-scale circulation changes due to aerosol forcing in regions far from the cloud cover change [*Rodwell and Jung*, 2008].

[64] We hypothesize that diabatic heating by absorbing aerosols in the rising branch of a direct circulation tends to enhance the ascent, increasing moisture convergence, low cloud cover (and even medium and high cloud cover), and precipitation depending on the strength of the radiative forcing in areas in which convection occurs. Highly reflecting aerosols at the same location would have the opposite effect on circulation, clouds, and precipitation. This occurs in our model during Northern Hemisphere summer over northeastern Africa, the Saudi Arabian Peninsula, and India and during Southern Hemisphere summer in the SPCZ. Our hypothesis is consistent with the “elevated heat pump” hypothesis that was formulated for the Asian summer monsoon [*Lau et al.*, 2006; *Lau and Kim*, 2006]. The response of the circulation in our simulations is also similar to results obtained with a quasi-equilibrium tropical circulation model

[Chou *et al.*, 2005] and a regional climate model covering western Africa [Solmon *et al.*, 2008].

[65] Conversely, radiative forcing by absorbing aerosols in the subsidence branch of a direct circulation weakens the circulation, whereas radiative forcing by strongly reflecting dust has the opposite effect. This occurs in our model during Northern Hemisphere winter, when the ITCZ is located south of the major dust regions of the Sahara, Sahel, and Saudi Arabian Peninsula.

[66] Since the magnitude and even the sign of the cloud cover response and the changes in the large-scale atmospheric circulation are sensitive to the absorptivity of aerosols, the radiative properties of soil dust particles, which vary with the source region, have to be precisely known to understand the climate effect of soil dust properly.

[67] Previous studies have shown that clouds below a dust layer increase the amount of radiation absorbed by aerosols, especially over the ocean with its low albedo [Chýlek and Coakley, 1974; Podgorny and Ramanathan, 2001; Keil and Haywood, 2003; Chand *et al.*, 2009]. Our results suggest the possibility of a positive feedback between increased cloud cover forced by absorbing aerosols and the amount of radiation absorbed in those regions. Whether such a feedback is present in our simulations has not been studied here and would require a more detailed analysis.

[68] A caveat is that the cloud cover increase in our simulations is related to the specific parameterizations in the model. For instance, the degree to which dust radiative forcing by absorbing aerosols enhances a direct circulation and increases cloud cover could be sensitive to the parameterized cloud changes in response to anomalous moisture convergence. Other studies using different GCMs with varied parameterizations are needed to test our results.

[69] In our simulations, we limited the effect of aerosols on clouds to radiative forcing. However, clouds are additionally modified by the microphysical effect of aerosols acting as CCN [Twomey, 1977; Albrecht, 1989; Pincus and Baker, 1994], giant CCN (GCCN) [Johnson, 1982; Feingold *et al.*, 1999], and ice-forming nuclei [Sassen, 2002; DeMott *et al.*, 2003]. These competing effects could counteract each other [Takemura *et al.*, 2007], or the microphysical effect of the tropospheric aerosols can act in the same direction as the radiative effect in our simulations; for example, dust acting as CCN can increase low cloud cover and suppress precipitation [Rosenfeld *et al.*, 2001; Mahowald and Kiehl, 2003; Twomey *et al.*, 2009]. On the other hand, large dust particles coated with soluble aerosols such as sulfate or sea salt acting as GCCN could enhance the formation of warm clouds that produce precipitation [Levin *et al.*, 1996; Levin *et al.*, 2005; van den Heever *et al.*, 2006; Cheng *et al.*, 2009], similar to the increase in cloud cover and precipitation in convective regions due to the radiative effect in our simulations.

[70] We suggest that the purely radiative effect of other absorbing aerosols such as black carbon on cloud cover, moisture, and the circulation will be qualitatively similar to the effect of the absorbing dust aerosols in our simulations, since the changes in these variables and the underlying physics do not depend on any assumptions about the microphysical properties of the aerosols such as the particle size, as long as these aerosols represent a sufficiently large source of radiative heating.

[71] **Acknowledgments.** We thank three anonymous reviewers for their constructive comments. This work was supported by grants ATM-01-34935 and ATM-06-20066 of the Climate Dynamics Program of the National Science Foundation and by the NASA Atmospheric Composition Program.

References

- Ackerman, A. S., O. B. Toon, D. E. Stevens, A. J. Heymsfield, V. Ramanathan, and E. J. Welton (2000), Reduction of tropical cloudiness by soot, *Science*, 288(5468), 1042–1047, doi:10.1126/science.288.5468.1042.
- Albrecht, B. A. (1989), Aerosols, cloud microphysics, and fractional cloudiness, *Science*, 245(4923), 1227–1230, doi:10.1126/science.245.4923.1227.
- Cairns, B., A. A. Lacis, and B. E. Carlson (2000), Absorption within inhomogeneous clouds and its parameterization in general circulation models, *J. Atmos. Sci.*, 57(5), 700–714, doi:10.1175/1520-0469(2000)057<0700:AWICAI>2.0.CO;2.
- Cess, R. D., G. L. Potter, S. J. Ghan, and W. L. Gates (1985), The climatic effects of large injections of atmospheric smoke and dust: A study of climate feedback mechanisms with one- and three-dimensional climate models, *J. Geophys. Res.*, 90(D7), 12,937–12,950, doi:10.1029/JD090iD07p12937.
- Chand, D., R. Wood, T. L. Anderson, S. K. Satheesh, and R. J. Charlson (2009), Satellite-derived direct radiative effect of aerosols dependent on cloud cover, *Nat. Geosci.*, 2(3), 181–184, doi:10.1038/ngeo437.
- Cheng, W. Y. Y., G. G. Carrió, W. R. Cotton, and S. M. Saleeby (2009), Influence of cloud condensation and giant cloud condensation nuclei on the development of precipitating trade wind cumuli in a large eddy simulation, *J. Geophys. Res.*, 114, D08201, doi:10.1029/2008JD011011.
- Chou, C., J. D. Neelin, U. Lohmann, and J. Feichter (2005), Local and remote impacts of aerosol climate forcing on tropical precipitation, *J. Clim.*, 18(22), 4621–4636, doi:10.1175/JCLI3554.1.
- Chýlek, P., and J. A. Coakley Jr. (1974), Aerosols and climate, *Science*, 183(4120), 75–77, doi:10.1126/science.183.4120.75.
- Cook, J., and E. Highwood (2004), Climate response to tropospheric absorbing aerosols in an intermediate general-circulation model, *Q. J. R. Meteorol. Soc.*, 130(596), 175–191, doi:10.1256/qj.03.64.
- Del Genio, A. D., and M. S. Yao (1993), Efficient cumulus parameterization for long-term climate studies: The GISS scheme, in *The Representation of Cumulus Convection in Numerical Models, Monograph*, vol. 24, edited by K. Emanuel and D. Raymond, pp. 181–184, Am. Meteorol. Soc., Boston, Mass.
- Del Genio, A. D., M.-S. Yao, W. Kovari, and K. K.-W. Lo (1996), A prognostic cloud water parameterization for global climate models, *J. Clim.*, 9(2), 270–304, doi:10.1175/1520-0442(1996)009<0270:APCWP>2.0.CO;2.
- DeMott, P. J., K. Sassen, M. R. Poellot, D. Baumgardner, D. C. Rogers, S. D. Brooks, A. J. Prenni, and S. M. Kreidenweis (2003), African dust aerosols as atmospheric ice nuclei, *Geophys. Res. Lett.*, 30(14), 1732, doi:10.1029/2003GL017410.
- Denman, K. L., et al. (2007), Couplings between changes in the climate system and biogeochemistry, in *Climate Change 2007: The Physical Science Basis—Contribution of Working Group I to the Fourth Assessment Report of the Intergovernmental Panel on Climate Change*, edited by S. Solomon et al., pp. 499–588, Cambridge Univ. Press, Cambridge, U. K.
- Dubovik, O., B. Holben, T. F. Eck, A. Smirnov, Y. J. Kaufman, M. D. King, D. Tanré, and I. Slutsker (2002), Variability of absorption and optical properties of key aerosol types observed in worldwide locations, *J. Atmos. Sci.*, 59(3), 590–608, doi:10.1175/1520-0469(2002)059<0590:VOAAOP>2.0.CO;2.
- Fan, J., R. Zhang, W.-K. Tao, and K. I. Mohr (2008), Effects of aerosol optical properties on deep convective clouds and radiative forcing, *J. Geophys. Res.*, 113, D08209, doi:10.1029/2007JD009257.
- Feingold, G., W. R. Cotton, S. M. Kreidenweis, and J. T. Davis (1999), The impact of giant cloud condensation nuclei on drizzle formation in stratocumulus: Implications for cloud radiative properties, *J. Atmos. Sci.*, 56(24), 4100–4117, doi:10.1175/1520-0469(1999)056<4100:TIOGCC>2.0.CO;2.
- Forster, P., et al. (2007), Changes in atmospheric constituents and in radiative forcing, in *Climate Change 2007: The Physical Science Basis—Contribution of Working Group I to the Fourth Assessment Report of the Intergovernmental Panel on Climate Change*, edited by S. Solomon et al., pp. 129–234, Cambridge Univ. Press, Cambridge, U. K.
- Grassl, H. (1975), Albedo reduction and radiative heating of clouds by absorbing aerosol particles, *Beitr. Phys. Atmos.*, 48, 199–209.
- Hansen, J., G. Russell, D. Rind, P. Stone, A. Lacis, S. Lebedeff, R. Ruedy, and L. Travis (1983), Efficient three-dimensional global models for climate studies: Model I and II, *Mon. Weather Rev.*, 111(4), 609–662, doi:10.1175/1520-0493(1983)111<0609:ETDGMF>2.0.CO;2.

- Hansen, J., M. Sato, and R. Ruedy (1997a), Radiative forcing and climate response, *J. Geophys. Res.*, *102*(D6), 6831–6864, doi:10.1029/96JD03436.
- Hansen, J., et al. (1997b), Forcing and chaos in interannual to decadal climate change, *J. Geophys. Res.*, *102*(D22), 25,679–25,720, doi:10.1029/97JD01495.
- Hansen, J., et al. (2002), Climate forcings in Goddard Institute for Space Studies SI2000 simulations, *J. Geophys. Res.*, *107*(D18), 4347, doi:10.1029/2001JD001143.
- Helmert, J., B. Heinold, I. Tegen, O. Hellmuth, and M. Wendisch (2007), On the direct and semidirect effects of Saharan dust over Europe: A modeling study, *J. Geophys. Res.*, *112*, D13208, doi:10.1029/2006JD007444.
- Hill, A. A., and S. Dobbie (2008), The impact of aerosols on non-precipitating marine stratocumulus, II: The semi-direct effect, *Q. J. R. Meteorol. Soc.*, *134*(634), 1155–1165, doi:10.1002/qj.277.
- Huang, J., B. Lin, P. Minnis, T. Wang, X. Wang, Y. Hu, Y. Yi, and J. K. Ayers (2006), Satellite-based assessment of possible dust aerosols semi-direct effect on cloud water path over East Asia, *Geophys. Res. Lett.*, *33*, L19802, doi:10.1029/2006GL026561.
- Hui, W. J., B. I. Cook, S. Ravi, J. D. Fuentes, and P. D'Odorico (2008), Dust-rainfall feedbacks in the West African Sahel, *Water Resour. Res.*, *44*, W05202, doi:10.1029/2008WR006885.
- Johnson, B. T., K. P. Shine, and P. M. Forster (2004), The semi-direct aerosol effect: Impact of absorbing aerosols on marine stratocumulus, *Q. J. R. Meteorol. Soc.*, *130*(599), 1407–1422, doi:10.1256/qj.03.61.
- Johnson, D. B. (1982), The role of giant and ultragiant aerosol particles in warm rain initiation, *J. Atmos. Sci.*, *39*(2), 448–460, doi:10.1175/1520-0469(1982)039<0448:TROGAU>2.0.CO;2.
- Keil, A., and J. M. Haywood (2003), Solar radiative forcing by biomass burning aerosol particles during SAFARI 2000: A case study based on measured aerosol and cloud properties, *J. Geophys. Res.*, *108*(D13), 8467, doi:10.1029/2002JD002315.
- Koren, I., Y. J. Kaufman, L. A. Remer, and J. V. Martins (2004), Measurement of the effect of Amazon smoke on inhibition of cloud formation, *Science*, *303*(5662), 1342–1345, doi:10.1126/science.1089424.
- Kubilyay, N., T. Cokacar, and T. Oguz (2003), Optical properties of mineral dust outbreaks over the northeastern Mediterranean, *J. Geophys. Res.*, *108*(D21), 4666, doi:10.1029/2003JD003798.
- Lacis, A. A., and M. I. Mishchenko (1995), Climate forcing, climate sensitivity, and climate response: A radiative modeling perspective on atmospheric aerosols, in *Aerosol Forcing of Climate*, edited by R. J. Charlson and J. Heintzenberg, pp. 11–42, John Wiley, New York.
- Lau, K.-M., and K.-M. Kim (2006), Observational relationships between aerosol and Asian monsoon rainfall, and circulation, *Geophys. Res. Lett.*, *33*, L21810, doi:10.1029/2006GL027546.
- Lau, K. M., M. K. Kim, and K. M. Kim (2006), Asian summer monsoon anomalies induced by aerosol direct forcing: The role of the Tibetan Plateau, *Clim. Dyn.*, *26*(7–8), 855–864, doi:10.1007/s00382-006-0114-z.
- Levin, Z., E. Ganor, and V. Gladstein (1996), The effects of desert particles coated with sulfate on rain formation in the eastern Mediterranean, *J. Appl. Meteorol.*, *35*(9), 1511–1523, doi:10.1175/1520-0450(1996)035<1511:TEODPC>2.0.CO;2.
- Levin, Z., A. Teller, E. Ganor, and Y. Yin (2005), On the interactions of mineral dust, sea-salt particles, and clouds: A measurement and modeling study from the Mediterranean Israeli Dust Experiment campaign, *J. Geophys. Res.*, *110*, D20202, doi:10.1029/2005JD005810.
- Mahowald, N. M., and L. M. Kiehl (2003), Mineral aerosols and cloud interactions, *Geophys. Res. Lett.*, *30*(9), 1475, doi:10.1029/2002GL016762.
- Menon, S., J. Hansen, L. Nazarenko, and Y. Lao (2002), Climate effects of black carbon aerosols in China and India, *Science*, *297*(5590), 2250–2253, doi:10.1126/science.1075159.
- Miller, R. L., and I. Tegen (1998), Climate response to soil dust aerosols, *J. Clim.*, *11*(12), 3247–3267, doi:10.1175/1520-0442(1998)011<3247:CRTSDA>2.0.CO;2.
- Miller, R. L., I. Tegen, and J. Perlwitz (2004), Surface radiative forcing by soil dust aerosols and the hydrologic cycle, *J. Geophys. Res.*, *109*, D04203, doi:10.1029/2003JD004085.
- Miller, R. L., et al. (2006), Mineral dust aerosols in the NASA Goddard Institute for Space Sciences ModelE atmospheric general circulation model, *J. Geophys. Res.*, *111*, D06208, doi:10.1029/2005JD005796.
- Mishra, S. K., and S. N. Tripathi (2008), Modeling optical properties of mineral dust over the Indian Desert, *J. Geophys. Res.*, *113*, D23201, doi:10.1029/2008JD010048.
- Patterson, E. M., and D. A. Gillette (1977), Commonalities in measured size distributions for aerosols having a soil-derived component, *J. Geophys. Res.*, *82*(15), 2074–2082, doi:10.1029/JC082i015p02074.
- Perlwitz, J., I. Tegen, and R. L. Miller (2001), Interactive soil dust aerosol model in the GISS GCM 1. Sensitivity of the soil dust cycle to radiative properties of soil dust aerosols, *J. Geophys. Res.*, *106*(D16), 18,167–18,192, doi:10.1029/2000JD900668.
- Pincus, R., and M. B. Baker (1994), Effect of precipitation on the albedo susceptibility of clouds in the boundary layer, *Nature*, *372*(6503), 250–252, doi:10.1038/372250a0.
- Podgorny, I. A., and V. Ramanathan (2001), A modeling study of the direct effect of aerosols over the tropical Indian Ocean, *J. Geophys. Res.*, *106*(D20), 24,097–24,105, doi:10.1029/2001JD900214.
- Ramanathan, V., et al. (2005), Atmospheric brown clouds: Impacts on South Asian climate and hydrological cycle, *Proc. Natl. Acad. Sci. U. S. A.*, *102*(15), 5326–5333, doi:10.1073/pnas.0500656102.
- Rodwell, M. J., and T. Jung (2008), Understanding the local and global impacts of model physics changes: An aerosol example, *Q. J. R. Meteorol. Soc.*, *134*(635), 1479–1497, doi:10.1002/qj.298.
- Rosenfeld, D., Y. Rudich, and R. Lahav (2001), Desert dust suppressing precipitation: A possible desertification feedback loop, *Proc. Natl. Acad. Sci. U. S. A.*, *98*(11), 5975–5980, doi:10.1073/pnas.101122798.
- Sassen, K. (2002), Indirect climate forcing over the western US from Asian dust storms, *Geophys. Res. Lett.*, *29*(10), 1465, doi:10.1029/2001GL014051.
- Satheesh, S. K., and K. K. Moorthy (2005), Radiative effects of natural aerosols: A review, *Atmos. Environ.*, *39*(11), 2089–2110, doi:10.1016/j.atmosenv.2004.12.029.
- Satheesh, S. K., and V. Ramanathan (2000), Large differences in tropical aerosol forcing at the top of the atmosphere and Earth's surface, *Nature*, *405*(6782), 60–63, doi:10.1038/35011039.
- Sokolik, I. N., and O. B. Toon (1999), Incorporation of mineralogical composition into models of the radiative properties of mineral aerosol from UV to IR wavelengths, *J. Geophys. Res.*, *104*(D8), 9432–9444, doi:10.1029/1998JD200048.
- Solmon, F., M. Mallet, N. Elguindi, F. Giorgi, A. Zakey, and A. Konaré (2008), Dust aerosol impact on regional precipitation over western Africa, mechanisms and sensitivity to absorption properties, *Geophys. Res. Lett.*, *35*, L24705, doi:10.1029/2008GL035900.
- Storelvmo, T., J. E. Kristjánsson, and U. Lohmann (2008), Aerosol influence on mixed-phase clouds in CAM-Oslo, *J. Atmos. Sci.*, *65*(10), 3214–3230, doi:10.1175/2008JAS2430.1.
- Sundqvist, H., E. Berge, and J. E. Kristjánsson (1989), Condensation and cloud parameterization studies with a mesoscale numerical weather prediction model, *Mon. Weather Rev.*, *117*(8), 1641–1657, doi:10.1175/1520-0493(1989)117<1641:CACPSW>2.0.CO;2.
- Takemura, T., Y. J. Kaufman, L. A. Remer, and T. Nakajima (2007), Two competing pathways of aerosol effects on cloud and precipitation formation, *Geophys. Res. Lett.*, *34*, L04802, doi:10.1029/2006GL028349.
- Tegen, I., and I. Fung (1995), Contribution to the atmospheric mineral aerosol load from land surface modification, *J. Geophys. Res.*, *100*(D9), 18,707–18,726, doi:10.1029/95JD02051.
- Tegen, I., and A. A. Lacis (1996), Modeling of particle size distribution and its influence on the radiative properties of mineral dust aerosol, *J. Geophys. Res.*, *101*(D14), 19,237–19,244, doi:10.1029/95JD03610.
- Tegen, I., P. Hollrig, M. Chin, I. Fung, D. Jacob, and J. Penner (1997), Contribution of different aerosol species to the global aerosol extinction optical thickness: Estimates from model results, *J. Geophys. Res.*, *102*(D20), 23,895–23,915, doi:10.1029/97JD01864.
- Trenberth, K. E., and C. J. Guillemot (1995), Evaluation of the global atmospheric moisture budget as seen from analyses, *J. Clim.*, *8*(9), 2255–2272, doi:10.1175/1520-0442(1995)008<2255:EOTGAM>2.0.CO;2.
- Twohy, C. H., et al. (2009), Saharan dust particles nucleate droplets in eastern Atlantic clouds, *Geophys. Res. Lett.*, *36*, L01807, doi:10.1029/2008GL035846.
- Twomey, S. (1977), The influence of pollution on the shortwave albedo of clouds, *J. Atmos. Sci.*, *34*(7), 1150–1152, doi:10.1175/1520-0469(1977)034<1149:TROPOT>2.0.CO;2.
- van den Heever, S. C., G. G. Carrió, W. R. Cotton, P. J. DeMott, and A. J. Prenni (2006), Impacts of nucleating aerosol on Florida storms. Part I: Mesoscale simulations, *J. Atmos. Sci.*, *63*(7), 1752–1775, doi:10.1175/JAS3713.1.
- Volz, F. E. (1973), Infrared optical constants of ammonium sulfate, Sahara dust, volcanic pumice, and flyash, *Appl. Opt.*, *12*(3), 564–568, doi:10.1364/AO.12.000564.
- Yanai, M., S. Esbensen, and J.-H. Chu (1973), Determination of bulk properties of tropical cloud clusters from large-scale heat and moisture budgets, *J. Atmos. Sci.*, *30*(4), 611–627, doi:10.1175/1520-0469(1973)030<0611:DOBPOT>2.0.CO;2.

R. L. Miller and J. Perlwitz, NASA GISS, 2880 Broadway, New York, NY 10025, USA. (rmiller@giss.nasa.gov; jperlwitz@giss.nasa.gov)